Structural and Functional Characterisation of the Human Mitochondrial Pyruvate Carrier

Simon Gripvall

Degree Project in Biochemistry, 2023
Department of Chemistry
Lund University
Sweden

MSc, 60 hp

LUND
UNIVERSITY

Structural and Functional Characterisation of the Human Mitochondrial Pyruvate Carrier

Simon Gripvall

LUND
UNIVERSITY

Degree Project in Biochemistry
2023
MSc, 60 hp

Supervisor:
Susanna Horsefield
Division of Biochemistry
and Structural Biology
Lund University
Sweden

Examiner:
Urban Johanson
Division of Biochemistry
and Structural Biology
Lund University
Sweden

Lund University
Department of Chemistry
Centre for Molecular Protein Science
P.O. Box 124
SE-221 00 Lund, Sweden

Popular science description

In cancer, type-II diabetes and neurological disorders, the way important molecules are interconverted into one another inside human cells is abnormally altered. An example of such a molecule is pyruvate. It is a central intermediary molecule in the processing of glucose that is present in the food we eat so we can generate energy for several important processes in the cell. A critical step in the continued processing of pyruvate is its transportation from the cytosol into the mitochondria. The protein responsible for this transportation is called the mitochondrial pyruvate carrier (MPC) and in humans, it consists of two different proteins (MPC1 and MPC2) cooperating and forming a complex to perform its function. It has been proposed that the MPC complex can serve as a potential drug target against the abovementioned diseases. Up until this point, there is no detailed information of how this protein is built up at a molecular level, which is required for efficient production of drugs. Moreover, it is also unclear of how many MPC1 and MPC2 proteins the MPC complex is composed of and which of three MPC complexes, MPC1 alone, MPC2 alone and MPC1/2 together is the main functional unit. The aim of this study is to investigate which of these three possible MPC complexes has the highest ability to transport pyruvate in a cell membrane resembling environment, called proteoliposomes, which are vesicles of lipid molecules in which the protein is imbedded in. The existence of a MPC1/2 complex, which several studies point towards is the main functional unit, was also examined with temperature stability tests based on the decomposition of the protein and with experiments in which one attempted to attach the two proteins together, called cross-linking. The detailed appearance of the MPC complex at a molecular level was supposed to be investigated as well, but due to lack of time this was not performed. To obtain these MPC1 and MPC2 proteins, cell membranes containing these proteins were extracted from yeast cells followed by isolation of the proteins with chromatographic methods based on their binding properties. It turned out that both MPC2 alone and MPC1/2 were able to actively transport pyruvate into these proteoliposomes, while MPC1 alone did not. In addition, the attempt to prove the existence of the MPC1/2 complex with the temperature stability tests as well as the attempt of cross-linking MPC1 and MPC2 together were both unsuccessful. In conclusion, although both MPC2 alone and MPC1/2 were able to transport pyruvate, it is still unclear which one of these two different species has the highest pyruvate transporting ability. Moreover, the unsuccessful attempt of the temperature stability tests as well as the cross-linking leaves the presence of the MPC1/2 heterocomplex still unknown and needs to be further investigated.

Abstract

The metabolism of pyruvate in the cell is abnormally regulated in several human diseases, such as type-II diabetes, cancer and neurodegenerative disorders, in which the human mitochondrial pyruvate carrier (HuMPC) sits at a pivotal point. It transports pyruvate across the inner mitochondrial membrane and consists of two proteins, MPC1 and MPC2, and is a potential drug target against these diseases. There is currently no three-dimensional structure at atomic resolution nor unambiguity of the biological oligomeric composition of this pyruvate transporting complex, although many studies advocate for a heterodimer of MPC1/2 being the main functional unit. In this study, the pyruvate transport activity of HuMPC complexes was investigated as well as the presence of a MPC1/2 heterocomplex. The pyruvate transport activity of human MPC1 alone, MPC2 alone and MPC1/2 mixed together was investigated with a proteoliposome assay based on the enzymatic activity of lactate dehydrogenase (LDH). In addition, the presence of the MPC1/2 complex in proteoliposomes was examined with nano-differential scanning fluorimetry, as well as with cross-linking trials for further analyses with mass spectrometry. Pure HuMPC protein was obtained by affinity chromatography from solubilised *Pichia pastoris* membranes. Here it was demonstrated that MPC2 and MPC1/2 displayed higher pyruvate transport activity compared to MPC1. Moreover, the nano-DSF measurement did not give any concrete evidence of the presence of the MPC1/2 heterocomplex. The mass spectrometric analyses did not identify any cross-links between MPC1 and MPC2 in the MPC1/2 proteoliposomes but more peptides of MPC2 than MPC1 could be identified. In conclusion, the true pyruvate transporting complex of HuMPC still remains unclear based on these results, as well as the existence of the MPC1/2 heterocomplex, which requires further investigation.

complex | MPC | proteoliposomes | pyruvate | transport

Acknowledgement

I would like to express my deepest gratitude to my co-supervisor, Tamim Al Jubair, for the tremendous supervision in the lab and for being a companion throughout this journey; to my main supervisor, Susanna Horsefield, for great supervision and outstanding input of experimental results as well as of this report; to Carl Johan Hagströmer and Helin Strandberg for great help around the lab and for gilding the many days of work; to my examiner, Urban Johanson, for incredible input of experimental results as well as for reviewing this report; to Balder Werin and Oliwia Kolodziejczyk for great brainstorming, help around the lab and good company throughout this adventure. I would also like to give many thanks to Katja Bernfur and Cecilia Emanuelsson for amazing help and work with the cross-linking and mass spectrometric analyses.

Table of contents

1 List of abbreviations

BSA	Bovine Serum Albumin
BSM	Basal Salt Medium
CV	Column Volume
DCP	Dodecylphosphocoline
DDM	n-Dodecyl-β-D-Maltopyranoside
DLS	Dynamic Light Scattering
DMSO	Dimethyl Sulfoxide
DO	Dissolved Oxygen
DSBU	Disuccinimidyl Dibutyric Urea
DSF	Differential Scanning Fluorimetry
EDTA	Ethylenediaminetetraacetic Acid
EM	Electron Microscopy
GFP	Green Fluorescent Protein
HuMPC	Human Mitochondrial Pyruvate Carrier
IMAC	Immobilised Metal Ion Affinity Chromatography
IMM	Inner Mitochondrial Membrane
IMS	Intermembrane Space
LDH	Lactate Dehydrogenase
LP3	Lund Protein Production Platform
LPR	Lipid-to-Protein Ratio

MES	2-(*N*-Morpholino)ethanesulphonic Acid
MD	Molecular Dynamics
MS	Mass Spectrometry
MWCO	Molecular Weight Cut-off
NADH	Reduced Nicotinamide Adenine Dinucleotide
ND	Not detected
NMR	Nuclear Magnetic Resonance
PMSF	Phenylmethylsulphonyl Fluoride
PPG	Polypropylene Glycol
PTM	*Pichia* Trace Metals
PVDF	Polyvinylidene Difluoride
SDS-PAGE	Sodium Dodecyl Sulphate Polyacrylamide Gel Electrophoresis
SEC	Size Exclusion Chromatography
SLC	Solute Carrier
TCEP	Tris(2-carboxyethyl)phosphine
TZDs	Thiazolidinediones
YPD	Yeast Extract-Peptone-Dextrose

2 Introduction

In several human physiological disorders, such as different types of cancer, type-II diabetes and various neurodegenerative diseases, the metabolism of the cell is abnormally altered. A pivotal part of this is the pyruvate metabolism (*1*,*2*,*3*,*4*,*5*) which joins amino acids, fatty acids and carbohydrates together. Pyruvate is a central branching point in several metabolic pathways and can therefore serve as a promising therapeutical treatment point. However, there are many enzymes that can metabolise pyruvate in various compartments which would require a cocktail of different therapeutical drugs. Furthermore, the cell is extraordinary in adapting to conditions when certain metabolites are depleted. A critical step for the anabolic and catabolic events of the cell is the pyruvate transport into the mitochondrial matrix. There is only one route for this which is through the mitochondrial pyruvate carrier (MPC) located in the inner mitochondrial membrane (IMM) (*6*). A more efficient way to counteract metabolic changes of pyruvate in the abovementioned diseases, would be to target the MPC which would enable to control whether pyruvate should be mainly in the cytosol or the mitochondrial matrix. This would shield pyruvate from a number of different enzymes in one of two major compartments depending on the situation, making it more challenging for the cell to find other pathways for compensating the pyruvate depletion.

Discovered in 2012 by two individual research groups (*7*,*8*), the human mitochondrial pyruvate carrier (HuMPC) was identified as being composed of two individual proteins, MPC1 and MPC2. MPC1 is 12 kDa with 109 amino acids and MPC2 is 14 kDa with 127 amino acids (*9*). Bricker *et al.* 2012 (*7*) showed that both MPC1 and MPC2 form a complex of 150 kDa with blue native polyacrylamide gel electrophoresis. However, Tavoulari *et al.* 2019 (*10*) contradicted this with that the Coomassie dye also binds to lipids and detergents in the ternary protein-lipid-detergent system, leading to that the protein contribution is roughly only 20 % of the total empirical mass in their study. This is also supported by Crichton *et al.* 2013 (*11*) in which they observe the same behaviour for various small membrane proteins. Bricker *el al.* 2012 (*7*) also demonstrated that MPC1 and MPC2 are adequate and essential for constituting a functional pyruvate transporting unit. However, it is still unclear whether these two proteins are the only ones constituting the MPC complex in a biological environment.

The transport of pyruvate into the mitochondrial matrix through MPC is coupled to symport with a proton, i.e., pyruvate and protons are transported through MPC in the same direction simultaneously and has been shown to be essential for pyruvate transport (*12*,*17*). Halestrap *et*

al. 1975 (*13*) demonstrated that both the pyruvate and proton transport are inhibited by a potent non-competitive inhibitor called UK 5099 with a K_i value of less than 1 μM and IC_{50} value of 50 nM. Another class of drugs, called thiazolidinediones (TZDs), has been demonstrated to also inhibit the MPC complex, although mildly, while exhibiting an insulin sensitising effect (*14*).

Although not fully established, numerous studies suggest that the main functional and most stable state of the HuMPC is a heterodimer of MPC1 and MPC2 determined with *in vitro* experiments and computational tools (*9,15,16*). Interestingly, Nagampalli *et al.* 2018 (*17*) demonstrated in their experimental setup that MPC2 alone could form homo-oligomers that were able to functionally transport pyruvate into proteoliposomes. Furthermore, they co-reconstituted MPC1 and MPC2 into proteoliposomes and obtained similar levels of pyruvate transporting ability as with MPC2 alone.

The MPC represents a subfamily of its own within the solute carrier (SLC) superfamily called SLC54A based on the functional properties of MPC (*18*). It is proposed that MPC is distantly related to a group of sugar efflux transporters from bacteria, the SemiSWEETs. This is based partly on their solute carrier functionality as well as their three-transmembrane topology (*9, 19*). However, the sequence identity between the SemiSWEETs and MPC proteins is rather low, only around 10%. The SemiSWEETs belong to the SLC50 subfamily as well as their eukaryotic homologues, the SWEETs (*19*). Xu *et al.* 2014 (*19*) determined the three-dimensional structure of two SemiSWEET isoforms from two different bacteria (Figure 1). Both form symmetrical and parallel homodimers with two three-transmembrane helical bundles, generating the sugar transporting pathway. Furthermore, one of the SemiSWEETs crystallised in an open state (Figure 1a) and the other in an occluded state (Figure 1b), which is indicating that they have a flip-flop type of movement during the transport in which they are open towards one side of the membrane and subsequently switches to being open towards the other side of the membrane. The presumably distant evolutionary relationship to the MPC may suggest that it could have the same flip-flop type of movement during transport of pyruvate. However, the MPC is thought to not form symmetrical dimers, but instead form asymmetrical dimers since pyruvate is an asymmetrical molecule, further advocating for the heterodimer of MPC as being the main functional unit since that would form an asymmetrical transport pathway as opposed to the homodimer (*18*).

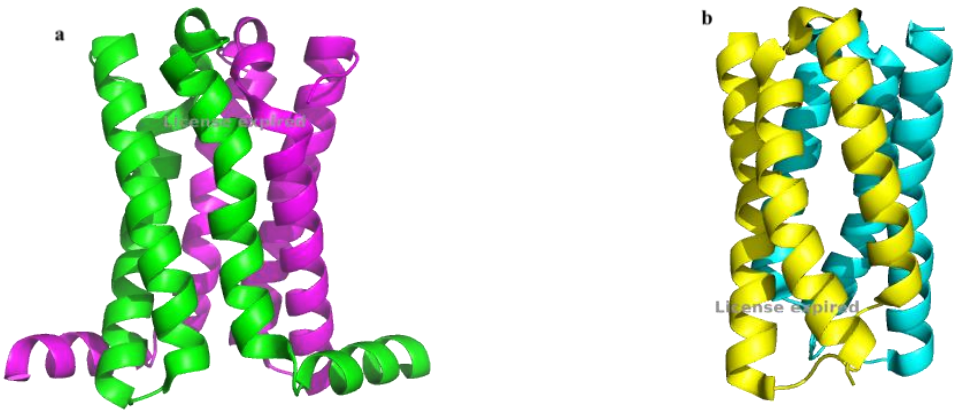

Figure 1: Structures of SemiSWEETs with the same topology viewed from the side of the membrane, (a) from *Vibrio* sp. N418 in which one protomer is coloured in green and the other in magenta, and (b) from *Leptospira biflexa* in which one protomer is shown in yellow and the other in cyan. The two pictures are generated in PyMOL from the PDB accession numbers 4QND in (a) and 4QNC in (b).

Xu *et al.* 2021 (*9*) proposed de novo models of the HuMPC1/2 heterodimer and performed all-atom molecular dynamics (MD) simulations in which they relaxed the structure in a lipid bilayer of the IMM. They propose that MPC1 and MPC2 have three transmembrane helices and an N-terminal amphipathic helix each which are exposed to the matrix side of the IMM (Figure 2). In Figure 2a, an inward-open conformation is shown of the MPC1/2 heterodimer, which is open towards the matrix, and in Figure 2b, an outward-open conformation is displayed opened towards the intermembrane space (IMS). This prediction is resembling the flip-flop movement that the SemiSWEETs are possessing and the overall topology is analogous to that of the SemiSWEETs as well. However, the relative positions of the transmembrane helices are disparate between the two proteins.

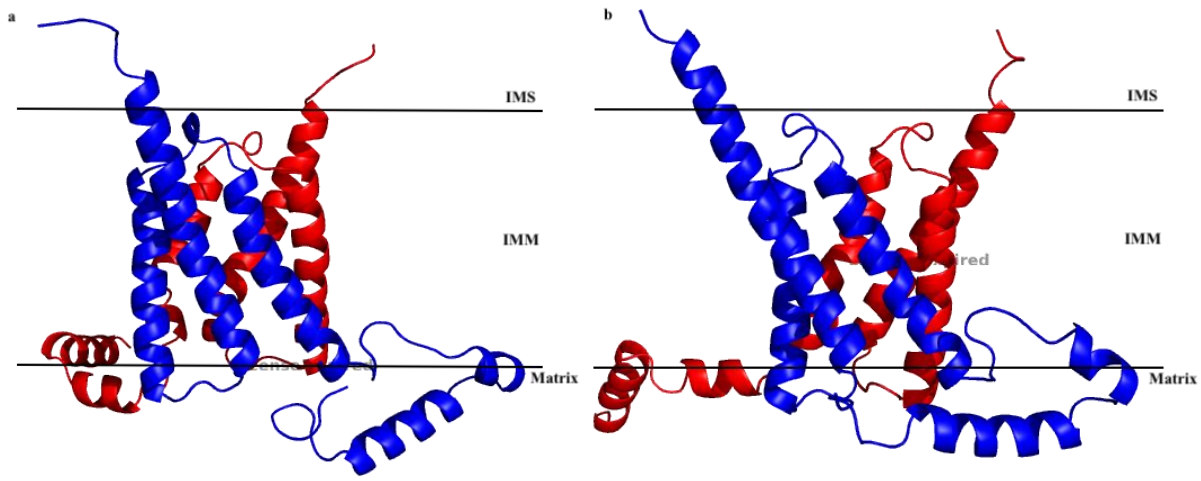

Figure 2: *De novo* models of the MPC1/2 heterodimer illustrated in the inner mitochondrial membrane (IMM) with the MPC1 monomer shown in red colour and the MPC2 monomer shown in blue colour, (a) in an inward-open conformation towards the mitochondrial matrix and (b) in an outward-open conformation towards the intermembrane space (IMS). The two pictures are generated in PyMOL from pdb files available in supporting information of Xu *et al.* 2021 (*9*).

The yeast homologue of MPC is also constituted of MPC1 and MPC2, however, a third subunit (MPC3) has been shown to be important for the function of MPC under certain conditions (*8,20*). Bender *et al.* 2015 (*20*) demonstrated that yeast growing during fermentative conditions, i.e., when the carbon source is glucose, MPC1 and MPC2 is the main functional unit termed MPC_{ferm}, while during respiratory conditions, i.e., when the carbon source is glycerol, MPC1 and MPC3 is the main functional unit termed MPC_{ox}. In that study, they state that MPC_{ox} has a higher pyruvate transport activity than MPC_{ferm} which is attributed due to the C-terminus of MPC3. The fate of intracellular pyruvate is shown to be regulated at the level of the MPC depending on the metabolic needs of the cell. In a study from 2019, Tavoulari *et al.* (*10*) identified that the main functional unit of yeast MPC is a heterodimer and that homodimers can be formed but they are non-functional. In another study from 2022, Li *et al.* (*21*) investigated the structural features of yeast MPC1 and MPC2 in dodecylphosphocoline (DCP) micelles using nuclear magnetic resonance (NMR) spectroscopy and demonstrated that both have three transmembrane helices. However, the structural experiments were performed on MPC1 and MPC2 individually and not in a stable complex and the researchers postulate that the reason could be that DCP is a rather strong detergent, blocking the interaction between the two proteins.

Currently there is no three-dimensional structure at atomic resolution of the HuMPC complex which would contribute with valuable information for drug development and for elucidating the mechanism of pyruvate transport. It would also remove ambiguity of the topology and stochiometric ratio of the HuMPC complex. Furthermore, uncertainty also lies in what the actual functional and biological unit of the HuMPC complex is which is able to transport pyruvate and if there are any additional proteins required in the proper complex formation in the cell.

The ultimate aim of this study is to determine the three-dimensional structure of the HuMPC complex using cryo-electron microscopy (cryo-EM). Furthermore, the aim is also to prove that

the purified HuMPC complex is functional using pyruvate transport assays with the protein incorporated into proteoliposomes and to demonstrate the existence of a heterocomplex consisting of MPC1 and MPC2 using nano-differential scanning fluorimetry (nano-DSF) and mass spectrometry (MS). Purified detergent-solubilised HuMPC is obtained from isolated *Pichia pastoris* membranes by affinity chromatography with poly-histidine and strep tags. Sodium dodecyl sulphate polyacrylamide gel electrophoresis (SDS-PAGE) and western blot were used to analyse purified protein and to assure successful incorporation of protein into proteoliposomes.

The basis of affinity chromatography is that the protein of interest containing some sort of purification tag, as a poly-histidine tag or a strep tag (which is a small peptide), can specifically interact strongly with a column resin containing a specific binding partner. Proteins absent of this purification tag do not bind into the column and thus get separated from the protein of interest. In the case of a poly-histidine tag, a column resin with immobilised Ni^{2+} ions is used which has a strong affinity for the imidazole group of histidine. This particular case is called immobilised metal ion affinity chromatography (IMAC) in which after a protein mixture containing the protein of interest with the purification tag has been applied to a Ni^{2+} column, impurities and loosely bound proteins are washed away with an increasing concentration of imidazole which competes for the binding spots with the Ni^{2+} ions. Finally the protein of interest is eluted with a high enough concentration of imidazole (usually 300 mM) which replaces the protein in the column and the protein is eluted and successfully isolated from a complex protein mixture. In the case of a strep tag, a column containing strep-tactin (which is an engineered streptavidin protein) is used which has a strong affinity for this small peptide, and the compound usually chosen to replace the bound protein of interest for elution is d-desthiobiotin. Here it is not necessary to wash away loosely bound proteins with an increasing concentration of d-desthiobiotin, but only with a suitable buffer absent of this compound in order to wash away unbound proteins. This is because the strep tag is rather more specific than the poly-histidine tag because some proteins might contain many histidines in their sequence and the strep tag is a synthetic peptide.

SDS-PAGE is an electrophoretic separation technique in which proteins denatured with SDS are migrating through a polyacrylamide mesh. The migration is caused by an applied electric field in which the negatively charged proteins are migrating from the negatively charged cathode to the positively charged anode. Since all proteins basically have the same negative

charge because of all the bound SDS, the proteins are separated on the basis of their molecular weights. Smaller proteins can migrate farther than larger proteins because of the increasing acrylamide cross-linking in the mesh, that is, the openings of the mesh become narrower and narrower the farther down the gel one migrates.

Western blot comprises the transfer of separated proteins by SDS-PAGE from the gel to some kind of membrane, usually polyvinylidene difluoride (PVDF) or nitrocellulose membranes. This is also caused by an electric field in which the negatively charged proteins transfer from the negatively charged cathode to the positively charged anode. This technique is used for a very sensitive detection method of a protein of interest containing a purification tag, such as poly-histidine tag or strep tag, involving the use of specific antibodies. The theory is that once the protein of interest has been transferred to the membrane, a so-called primary antibody of a certain specificity towards a certain purification tag is applied. The antibody is present in usually either non-fat milk powder or bovine serum albumin (BSA) which ascertains specific binding of the antibody to the protein of interest with the purification tag since the proteins in the non-fat milk powder or BSA are binding non-specifically to all proteins present on the membrane. Subsequently, a secondary antibody also present in non-fat milk powder or BSA is applied onto the membrane which has a specific affinity for the primary antibody. The secondary antibody is usually fused to an enzyme that catalyses a chemiluminescent reaction in which a substrate is converted to a product that luminates light, hence, enabling the specific detection of the protein of interest.

Proteoliposomes are unilamellar lipid vesicles with the protein imbedded in the lipid bilayer. The basis for the proteoliposome formation in this study is that one starts with a thin lipid film which is dried from chloroform, from which multilamellar lipid-detergent micelles spontaneously form when resuspending the film in a buffer containing a mild detergent. To homogenise the lipid-detergent mixture, heating and sonication is performed, which forms small unilamellar vesicles. When the detergent-solubilised membrane protein is added, a ternary protein-lipid-detergent mixture is formed. For full reconstitution of the protein, a number of freeze-thaw cycles are performed, which forms large unilamellar vesicles from fusion of small unilamellar vesicles, followed by sonication, which again forms small unilamellar vesicles. The final step to allow proteoliposomes to form is the removal of the detergent, which is performed by adsorption of the detergent to polystyrene beads. Here it is the lipids that replaces the detergent to keep the membrane protein still soluble and not

aggregating. The proteoliposomes are then extruded through a polycarbonate filter which allows the formation of uniform vesicles, that is, vesicles with similar sizes. These proteoliposomes are a great system for studying the function of membrane proteins since it is mimicking biological membranes quite well and allows for the elimination of unknown factors, such as other proteins in a complex biological environment, affecting the results of the studies.

Nano-DSF is a technique in which it determines the thermal stability of proteins. A temperature gradient is applied, and while the protein gradually unfolds, the residues of the protein become more exposed, especially hydrophobic ones that are buried in the core of the protein. In this technique, the fluorescence of aromatic residues (especially of tryptophan) is measured and when the protein is unfolding and these residues become more exposed, the fluorescence is increased. At the temperature when the protein starts to unfold is called the onset temperature. The temperature at the centre-point of an unfolding event is called an inflection point or the melting temperature, and the higher this temperature is, the more thermally stable is the protein.

3 Materials and Methods

3.1 Overproduction of HuMPC in *Pichia pastoris*

Worked under sterile conditions. One construct of human *mpc1* with a C-terminal strep tag and one construct of human *mpc2* with a C-terminal 8x-his tag in *Pichia pastoris* (*P. pastoris*), both with the AOX1 promoter, were separately streaked on yeast extract-peptone-dextrose (YPD) agar plates [1% (w/v) yeast extract, 2% (w/v) peptone, 2% (v/v) dextrose and 2% (w/v) agar]. Plates were incubated at 30°C over three nights and subsequently stored at 4°C until further use. Following procedure was performed on the *mpc1* construct and *mpc2* construct separately. *P. pastoris* cells from the plate with the *mpc1* or *mpc2* construct were resuspended in 100 mL YPD medium [1% (w/v) yeast extract, 2% (w/v) peptone, 2% (v/v) dextrose] and were grown at 30°C overnight. The cell suspension was transferred to a 3 L fermentor (Belach Bioteknik AB) containing 1.5 L basal salt medium (BSM) [0.093% (w/v) calcium sulphate, 1.82% (w/v) potassium sulphate, 1.49% (w/v) magnesium sulphate 7 × H_2O, 0.41% (w/v) potassium hydroxide, 4.02% (w/v) glycerol, 2.67% (v/v) phosphoric acid]. This was supplemented with 6.5 mL *Pichia* trace metals (PTM) [0.6% (w/v) cupric sulphate, 0.008% (w/v) sodium iodide, 0.3% (w/v) manganese sulphate × H_2O, 0.02% (w/v) sodium molybdate 2 × H_2O, 0.002% (w/v) boric acid, 0.05% (w/v) cobalt chloride, 2% (w/v) zinc chloride, 6.5% (w/v) ferrous sulphate 7 × H_2O, 0.02% (w/v) biotin, 0.5% (w/v) sulphuric acid]. A few drops of 50% (w/v) polypropylene glycol (PPG) P2000 was added as an anti-foam agent when necessary during the overproduction. The fermentor was run overnight at 30°C, pH 5.0-5.1 maintained with 1M hydrochloric acid (HCl) and 25% ammonium hydroxide, and the dissolved oxygen (DO) at 25, until the glycerol was depleted. The cells continued to grow with 200 mL of 50% (v/v) glycerol supplemented with 2.4 mL PTM and subsequently switched to 400 mL of pure methanol supplemented with 4.8 mL PTM, starting the induction of MPC overexpression. Methanol is the choice of inducer since the *mpc1* and *mpc2* genes are under the control of the AOX1 promoter. After induction over two nights, the cells were harvested by centrifugation in a JLA-8.1000 rotor (Beckman Coulter) at 9,000 × *g* at 4°C for 25 min. The pelleted cells were stored at -80°C until further use.

3.2 Cell breaking and membrane isolation

The procedure was performed for HuMPC1 and HuMPC2 individually. To 100 g of frozen *P. pastoris* cells was added 100 mL of breaking buffer [50 mM potassium phosphate pH 7.5, 5%

(v/v) glycerol, 2 mM ethylenediaminetetraacetic acid (EDTA)] and the cells were thawed while stirring. The resulting cell suspension was supplemented with 1 mM phenylmethylsulphonyl fluoride (PMSF) and mixed with 200 mL of glass beads (0.5 mm, Techtum) in a stainless-steel chamber jar (350 mL, BioSpec Products) for bead beating with a Bead Beater HAMILTON BEACH 908 BASE (BioSpec Products). The bead beater was run at 30 × 30 seconds rounds with 30 seconds pause between each round. After removal of the broken cells, the glass beads were washed with 100 mL of breaking buffer to increase the recovery of broken cells. Large cell debris and unbroken cells were pelleted by centrifugation in a JLA-10.500 rotor (Beckman Coulter) or a JA-14 rotor (Beckman Coulter) at 17,000 × *g* or 14,000 × *g*, respectively, at 4°C for 40 min. The isolation of the membranes in the supernatant was performed by ultracentrifugation in a Ti-45 rotor (Beckman Coulter) at 235,000 × *g* at 4°C for 1h. The pelleted membranes were homogenised in a potter homogeniser with urea buffer [5 mM Tris pH 9.5, 4M urea, 2 mM EDTA] in order to remove peripheral membrane proteins. The washed membranes were pelleted by ultracentrifugation in a Ti-45 rotor (Beckman Coulter) at 235,000 × *g* at 4°C for 2h. The pelleted membranes were homogenised in a potter homogeniser with membrane buffer [20 mM Tris pH 8.0, 20 mM NaCl, 10% (v/v) glycerol] supplemented with 1 mM PMSF and 2 mM EDTA in order to remove the urea. The washed membranes were pelleted by ultracentrifugation in a Ti-45 rotor (Beckman Coulter) at 235,000 × *g* at 4°C for 1h and 15 min. The pelleted membranes were homogenised in a potter homogeniser with 1 mL membrane buffer/g membrane, flash frozen in liquid nitrogen and stored at -80°C until further use. Alternatively, the cells were broken using a French press at 1000 psi passing the cells through three times in total, when the bead beater was unavailable for use.

3.3 Solubilisation and purification

The procedure was performed either for HuMPC1 C-terminal strep tag and HuMPC2 C-terminal 8xHis together or individually. Procedure for two-step purification of HuMPC1 and HuMPC2 together: Crudely purified membranes of HuMPC1 and HuMPC2 were mixed together with solubilisation buffer [20 mM Tris pH 8.0, 300 mM NaCl, 2% (w/v) n-dodecyl-β-D-maltopyranoside (DDM)] at a 1:1 volume ratio supplemented with 1 mM PMSF. The proteins were solubilised at a final concentration of 1% (w/v) DDM at 4°C for 2h under gentle rotation. The lipids of the membranes were removed by centrifugation in a JA-25.50 rotor (Beckman Coulter) at 56,000 × *g* at 4°C for 1h and 30 min supplemented with 1 mM PMSF. All buffers in the following procedure were degassed and filtered through nitrocellulose

membrane (0.45 μm, Cytiva) and the purifications were performed on an NGC chromatography system (Bio-Rad). The solubilised proteins were loaded on a HisTrap HP pre-packed 5 mL column (Cytiva) at 0.8 mL/min equilibrated with 4 column volumes (CV) of binding buffer [20 mM Tris pH 8.0, 300 mM NaCl, 5% (v/v) glycerol, 0.05% (w/v) DDM]. The column was washed with 4 CV of binding buffer supplemented with 50 mM imidazole and subsequently with 4 CV of binding buffer supplemented with 100 mM imidazole in order to remove unbound and loosely bound protein. The protein was eluted with 4 CV of binding buffer supplemented with 300 mM imidazole. Eluted protein was desalted with binding buffer using a disposable PD-10 desalting column (Cytiva) and subsequently loaded on a StrepTrap HP pre-packed 5 mL column (Cytiva) at 0.5 mL/min equilibrated with 4 CV of binding buffer. The column was washed with 4 CV of binding buffer in order to remove unbound protein. The protein was eluted with 4 CV of binding buffer supplemented with 2.5 mM d-desthiobiotin. Eluted protein was desalted with binding buffer using a disposable PD-10 desalting column (Cytiva) and the protein concentration was subsequently increased to using a Vivaspin 6 concentrator (Sartorius) with a 10 kDa molecular weight cut-off (MWCO). Alternatively, HuMPC1 and HuMPC2 together were purified first through the StrepTrap HP pre-packed 5 mL column (Cytiva) and subsequently through the HisTrap HP pre-packed 5 mL column (Cytiva), or one-step purified through either column, with the same procedure as above. The purified protein was analysed, when necessary, with SDS-PAGE and western blot using the XCell system (Invitrogen). For SDS-PAGE, NuPAGE 4 to 12%, Bis-Tris, 1.0–1.5 mm, Mini Protein Gels (Thermo Scientific) were used and for western blot, Amersham Protran Western blotting membranes, nitrocellulose (Cytiva) were used. The protein standard that was used is Spectra Multicolor Broad Range Protein Ladder (Thermo Scientific). Furthermore, the purified protein was analysed with Blue Native-PAGE using the Novex Bis-Tris gel system (Invitrogen) and NativePAGE 3 to 12%, Bis-Tris, 1.0 mm, Mini Protein Gels (Thermo Scientific). The protein standard that was used is NativeMark Unstained Protein Standard (Thermo Scientific). The purified protein was used immediately for further studies or flash frozen in liquid nitrogen and stored at -80°C until further use. The same procedure as above was used for one-step purification of HuMPC1 and HuMPC2 individually through their respective column based on their purification tags.

3.4 Proteoliposome preparation

The procedure explained here originates from previously described protocols (*17,22*). Asolectin from soybean dissolved in pure chloroform was dried into a thin lipid film using a weak stream

of gaseous N_2 and was further dried in a vacuum desiccator overnight. The dried lipid film was resuspended in lipid-resuspension buffer [20 mM Tris pH 8.0, 300 mM NaCl, 5% (v/v) glycerol, 0.5 mM tris(2-carboxyethyl)phosphine (TCEP), 0.03% (w/v) DDM] and subsequently heated at 70°C for 1h while vortexing every 10 min. The lipid suspension was sonicated in a water-bath sonicator for three cycles of 15 min on/5 min off to obtain a homogenous lipid-detergent mixture. Purified protein in the form of HuMPC1 alone, HuMPC2 alone, and HuMPC1/2 pre-incubated for a minimum of 1h on ice together at a 1:1 mole ratio from individually purified HuMPC1 and HuMPC2, were each added separately to a lipid-detergent aliquot at a lipid-to-protein (LPR) ratio of 10:1 (w/w). As a control sample, empty liposomes with no protein incorporated were also prepared in the same manner with the addition of binding buffer instead of the protein solution. The ternary protein-lipid-detergent mixture was flash frozen in liquid nitrogen and thawed for three cycles to obtain full reconstitution and subsequently sonicated as described above. The detergent was removed with the addition of Amberlite XAD-2 (Supelco), which are polystyrene beads, at 1 g beads/mL solution and incubated at 4°C overnight, allowing the formation of proteoliposomes and liposomes. Before addition, the polystyrene beads were activated by washing once with pure methanol, twice with pure ethanol, followed by five times with Milli-Q water and finally three times with lipid-resuspension buffer. After removal of the polystyrene beads, the proteoliposomes/liposomes were pelleted by ultracentrifugation using an Airfuge (Beckman Coulter) at 20 Psig (~100,000 × *g*) for 45 min. The pelleted vesicles were resuspended in liposome-resuspension buffer [20 mM Tris pH 8.0, 300 mM NaCl, 5% glycerol, 0.5 mM TCEP] and subsequently extruded 15 times, for a uniform particle size distribution, through a polycarbonate membrane (100 nm pore diameter, Avestin) equilibrated with liposome-resuspension buffer. The extruded vesicles were analysed using dynamic light scattering (DLS) to verify the uniform particle size distribution and also with SDS-PAGE and western blot to verify protein incorporation into the proteoliposomes. Furthermore, the concentration of the proteoliposomes/liposomes was increased, for the nano-DSF and cross-linking experiments in section 3.6, using a Pierce Protein Concentrator (Thermo Scientific) with a 30 kDa MWCO.

3.5 Pyruvate transport activity assay

The procedure explained here originates from a previously described protocol (*17*). The assay was performed at room temperature and in triplicates. Transport of pyruvate into the proteoliposomes/liposomes with an internal pH of 8.0 was initiated by mixing 50 µL of the

proteoliposomes/liposomes with 100 µL of transport buffer [100 mM 2-(*N*-morpholino)ethanesulfonic acid (MES) pH 6.5, 120 mM KCl, 50 µM sodium pyruvate]. So, pyruvate and protons are co-transported into the proteoliposomes/liposomes in the presence of a pH gradient of 1.5 across the lipid bilayer. After certain incubation times of 1, 3, and 5 min, 50 µL of stop buffer [50 mM Tris pH 8.0, 0.5 mM NADH, 2 nM L-LDH from rabbit muscle] was added which stops the pyruvate transport since the pH gradient is abolished. Immediately after addition, the absorbance of the mixture was quantified at 340 nm on a 96-well plate reader to track how much of the NADH that had been oxidised. In addition, the same procedure was performed in the absence of proteoliposomes/liposomes, i.e., only with liposome-resuspension buffer. Unpaired Student's *t*-tests were performed to prove the presence or absence of a statistically significant difference of the pyruvate transport between the HuMPC proteoliposomes/liposomes.

3.6 Nano-DSF and cross-linking for mass spectrometry

The empty liposomes and proteoliposomes containing HuMPC1 alone, HuMPC2 alone, and HuMPC1/2 together were analysed for temperature stability with nano-DSF measuring the intrinsic fluorescence of the proteins using Prometheus NT.48 (NanoTemper) at the Lund Protein Production Platform (LP3). The proteoliposomes/liposomes were loaded into high sensitivity capillary tubes and subjected to a temperature gradient of 1°C/min from 20 to 95°C. Furthermore, a cross-linking experiment was performed on the proteins in these proteoliposome samples using a ~12.5 Å long membrane permeable cross-linker, disuccinimidyl dibutyric urea (DSBU), dissolved in dimethyl sulfoxide (DMSO). DSBU was added at a cross-linker to protein ratio of 133:1. The mixture was incubated on ice for 30 min and the reaction was stopped with the addition of 20 mM Tris pH 8 followed by incubation on ice for 15 min. The proteoliposomes used for this cross-linking experiment was prepared in a 20 mM HEPES pH 8.0 buffer, instead of Tris, since Tris buffer is not compatible with DSBU as a cross-linker. The cross-linked samples were analysed with SDS-PAGE and the proteins were detected with the Pierce Silver Stain for Mass Spectrometry kit (Thermo Scientific). The gel was handed to Katja Bernfur (research engineer, Biochemistry and Structural Biology, Lund University) for in-gel digestion of the protein by trypsin at the C-terminal end of lysine and arginine residues, and finally mass spectrometric analysis of the peptides in the cross-linked samples. The identification of peptides was performed using the Mascot database of protein sequences.

4 Results and discussions

4.1 Purification of the HuMPC1/2 heterocomplex

To obtain pure HuMPC protein, *Pichia Pastoris* cells that were grown in a fermentor, in which the MPC proteins were overexpressed under the control of the AOX1 promoter with methanol as inducer, were broken using a bead beater with the subsequent isolation of the membrane fraction using ultracentrifugation. The MPC1 and MPC2 proteins were extracted from the membrane fraction with detergent and the heterocomplex of MPC1/2 was attempted to be two-step purified by affinity chromatography with HisTrap and StrepTrap columns in which MPC2 is supposed to bind to the HisTrap column with its his tag and MPC1 to the StrepTrap column with its strep tag while the two proteins are supposedly interacting with each other. Figure 3 and 4 illustrate elution profiles of purified HuMPC1/2 heterocomplex when the MPC2 protein is binding to the HisTrap column and the MPC1 protein is binding to the StrepTrap column, respectively. The heterocomplex eluted from the HisTrap column at ~1.5 CV after the addition of 300 mM imidazole and as can be seen in Figure 3, the plateau of the elution peak is probably caused by the high concentration of imidazole, which has quite a high absorbance at 280 nm, relative to the protein amount that is eluting. The eluted heterocomplex from the HisTrap was loaded on the StrepTrap column and eluted at ~1.5 CV after the addition of 2.5 mM d-desthiobiotin. The oscillating profile from fraction A10 to A24 during the washing of the column in Figure 3 is likely due to insufficient degassing of the binding buffer. The elution profiles of other purifications described in section 3.3 are similar to those in Figure 3 and 4 (data not shown).

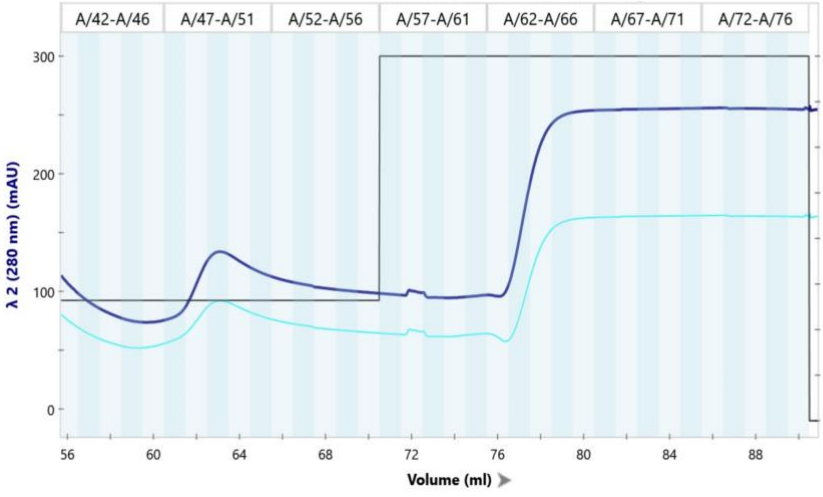

Figure 3: Elution profile of purified HuMPC1/2 heterocomplex through the MPC2 protein with a HisTrap column. The y- and x-axis show the absorbance at 280 nm in milli absorbance units (mAU) and volume passing through the column in millilitre (mL), respectively. The dark and light blue lines follow the absorbance at 280 and 260 nm, respectively. The black line follows the percentage of 300 mM imidazole passing through the column.

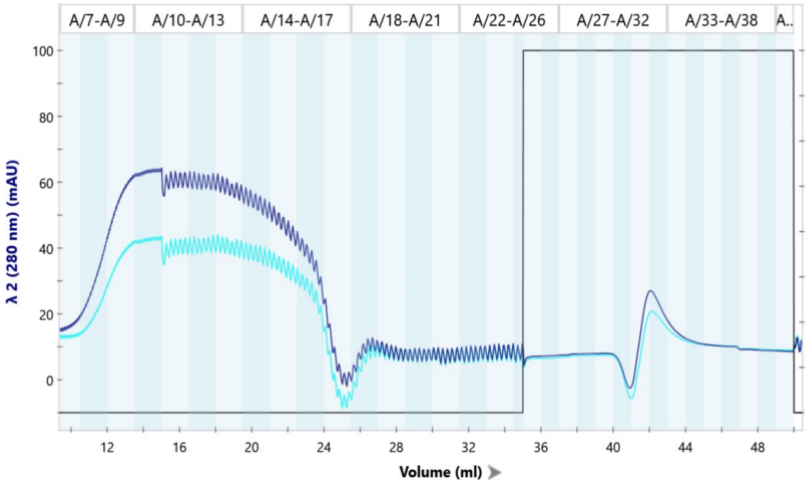

Figure 4: Elution profile of purification of HuMPC1/2 heterocomplex through the MPC1 protein with a StrepTrap column after the HisTrap purification. The y- and x-axis show the absorbance at 280 nm in milli absorbance units (mAU) and volume passing through the column in millilitre (mL), respectively. The dark and light blue lines follow the absorbance at 280 and 260 nm, respectively. The black line follows the percentage of 2.5 mM d-desthiobiotin passing through the column.

Figure 5 demonstrate western blots of samples from the attempt of two-step purifying the heterocomplex HuMPC1/2 first through the HisTrap and subsequently through the StrepTrap. In Figure 5a and 5b, the MPC2 protein with its his tag at around the expected 15 kDa range and MPC1 protein with its strep tag also around the expected 15 kDa range is detected, respectively. What can be noticed is that MPC2 is detected until the elution from the StrepTrap in Figure 5a and MPC1 is not detected until after the desalting of the eluate from the StrepTrap in Figure 5b. It seems that MPC2 and MPC1 are making an interaction with each other since MPC1 is detected in Figure 5b after passing through first the HisTrap, in which MPC2 binds into the column, and then the StrepTrap, in which MPC1 is binding into the column. Figure 6 shows the western blots of samples from a one-step purification of HuMPC1/2 through StrepTrap. The MPC2 and MPC1 protein is detected in Figure 6a and 6b, respectively. Notice that in HuMPC1/2 after StrepTrap the MPC1 is detected as expected in Figure 6b, however, traces of

MPC2 are detected in Figure 6a. The MPC2 signal did not appear at first (data not shown), but with more exposure of the membrane, the signal appeared as can be seen in Figure 6a.

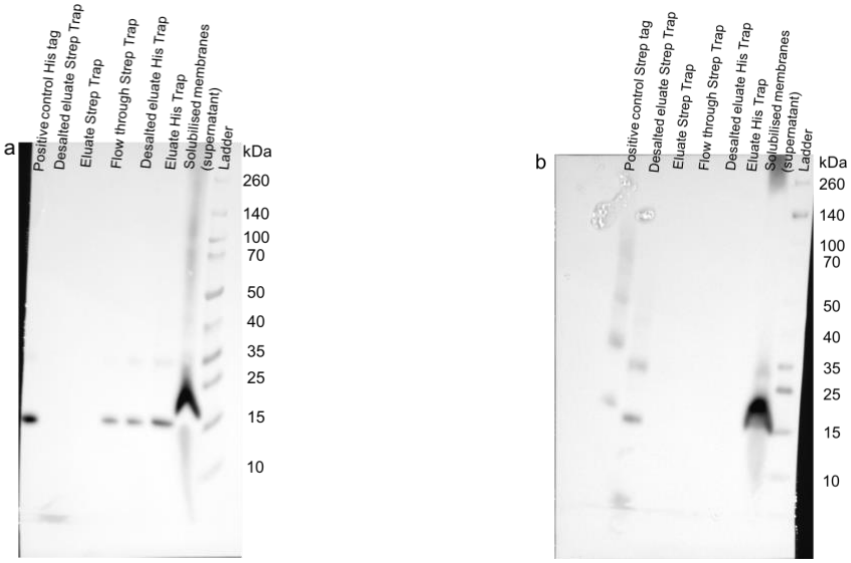

Figure 5: Western blot of attempted two-step purification of the heterocomplex HuMPC1/2 first through HisTrap and then StrepTrap. Above each well there is an explanation of what sample has been loaded. In (a), antibody against his tag has been used and the positive control for his tag is individually purified HuMPC2. In (b), antibody against strep tag has been used and the positive control for strep tag is purified CEHRG4 provided by supervisors. Pictures were generated with a Gel Imaging System (Syngene).

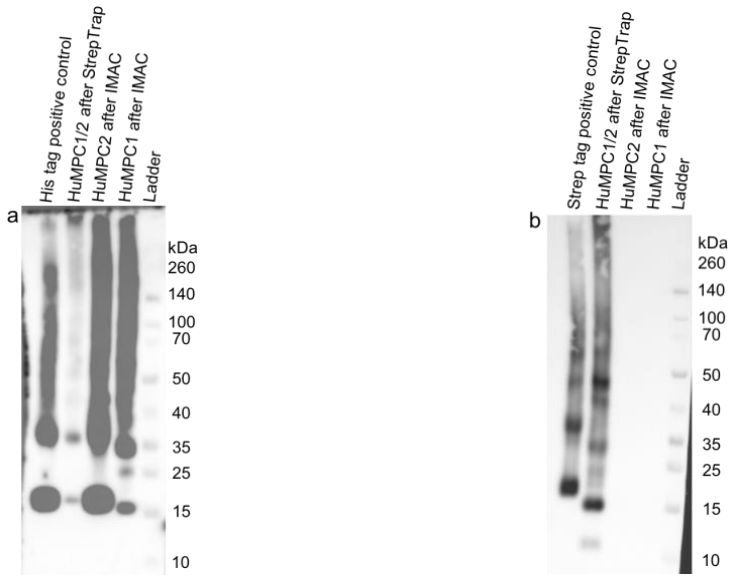

Figure 6: Western blot of one-step purified heterocomplex of HuMPC1/2 through StrepTrap. Above each well there is an explanation of what sample has been loaded. In (a), antibody against his tag has been used and the positive control for his tag is individually purified HuMPC2. In (b), antibody against strep tag has been used and the positive control for strep tag is purified CEHRG4 provided by supervisors. Pictures were generated with a Gel Imaging System (Syngene).

Altogether, when one-step purifying the heterocomplex HuMPC1/2, traces of the binding partner is accompanied with the protein that binds into the column which suggests that an interaction is present although rather weak. The reason to this could be due to the detergent that maintains the protein stable in solution. The detergent used here, DDM, is a rather long-chained detergent with a 12-carbon long chain as its hydrophobic part. Furthermore, it has a rather large hydrophilic sugar moiety as well. This creates a rather large detergent micelle around the protein which could shield parts of the protein important for interaction with its partner. Another reason could be that since no triple deleted *mpc1, mpc2 and mpc3* mutant *P. pastoris* strain was used, endogenous MPC subunits could have co-purified with the HuMPC subunits, already forming a complex which could prevent the HuMPC subunits to form complexes with each other. When attempting to two-step purify the HuMPC1/2, an interaction between MPC2 and MPC1 is present as discussed above, however, it is rather strange that MPC2 is not detected at all in the desalted eluate from StrepTrap in Figure 5a since it was detected in the desalted eluate from HisTrap. Notice that a prominent signal of MPC2 is present in the flow-through from StrepTrap which is probably MPC2 monomers not in a complex with MPC1 further indicating the weak interaction between them in this experimental setup. A possible explanation to why not even traces of MPC2 is visible in the desalted eluate from StrepTrap in Figure 5a is that the exposure from the camera in the imaging system was adjusted to the stronger bands so they do not get overexposed. It is likely that if one manually overexposed the membrane in Figure 5a, traces of MPC2 would have been detected. Nagampalli *et al.* 2018 (*17*) demonstrated that when purifying the HuMPC1/2 heterocomplex in yeast through MPC1, co-expressed with MPC2, trace amounts of MPC2 were observed to co-purify. Furthermore, they used DDM as detergent and this outcome is resembling to the obtained results in this study. Lee *et al.* 2020 (*15*) demonstrated that when purifying HuMPC1/2 in insect cells through MPC1, co-expressed with MPC2, the MPC2 protein was more abundant than MPC1 with Coomassie staining and they also used DDM as detergent. The authors of that paper reason that the cause to this observation could be the low content of aromatic residues in MPC1 relative to MPC2. However, the authors do not explain in what way this would affect the MPC1 signal on the Coomassie stained gel, but it could be that the Coomassie is interacting hydrophobically with aromatic groups like tryptophan, tyrosine and phenylalanine (*23*), resulting in less Coomassie being able to bind to MPC1 relative to MPC2. Nagampalli *et al*. 2018 (*17*) argue that the reason only trace amounts of MPC2 co-purified with MPC1 in their study could be that yeast does not possess additional factors such as certain proteins, lipids or small molecules for a stable complex formation of human MPC1/2 to take place. Indeed, insect cells have a more similar environment, natively

speaking, to human cells in comparison to yeast cells. This could be another reason for the increased complex formation of HuMPC1/2 in the study conducted by Lee *et al*. 2020 (*15*).

4.2 Blue Native-PAGE of human MPC1, MPC2 and MPC1/2 complexes

The apparent molecular weight of the HuMPC complexes in this study was attempted to be determined by Blue Native-PAGE. Figure 7 shows western blots after Blue Native-PAGE of one-step purified HuMPC1/2 through StrepTrap, and individually purified HuMPC2 and HuMPC1 both with his tags through IMAC. As can be seen in both blots, there is some migration although very smeary. In Figure 7a, MPC2 is not detected in the heterocomplex MPC1/2, but MPC1 is detected in Figure 7b because of reasons discussed in section 4.1. It seems like most of the protein in the samples cannot migrate in the gel which can be seen from the black colour in the bottom of the wells. This could be due to that the protein in the samples is aggregated, however, no indication of this has been present at any other time. Furthermore, according to the user guide manual of this Blue Native-PAGE system, high salt concentration in the samples can cause this smeary appearance and they recommend using 50 mM NaCl, different from the 300 mM NaCl in this study. Based on the appearance in the two blots, too much protein seems to have been loaded since in the bottom of the wells in Figure 7a and close to the well HuMPC1/2 after StrepTrap in Figure 7b, there is strong signals, contributing to the smeary appearance. Another contributing factor to the abnormal migration of the proteins could be that the gel used in this experiment was expired, but to what extent this would have affected is ambiguous. The faint bands of HuMPC1/2 after StrepTrap in Figure 7a and of HuMPC1 after IMAC in Figure 7b are most likely due to artefacts of the dye front since his tags should not be detected in Figure 7b because antibody against strep tag was used. Unfortunately, the bands of the ladder are not visible on the western blots since an unstained protein standard was used which also is not chemiluminescent, so, the sizes of the proteins in the ladder cannot be assigned accurately on the blot.

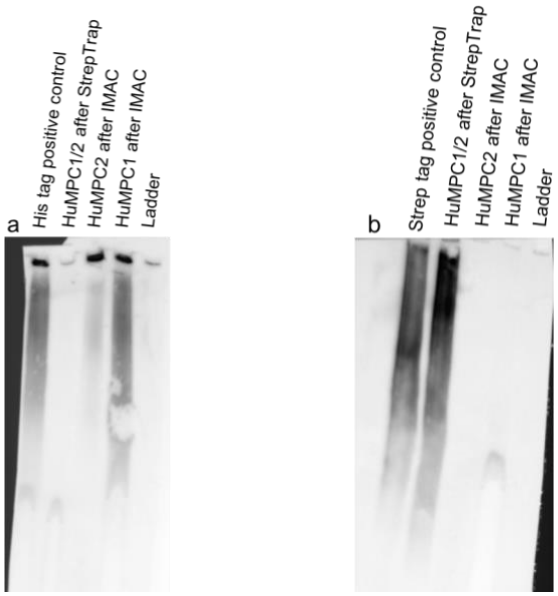

Figure 7: Western blot after Blue Native-PAGE of one-step purified heterocomplex of HuMPC1/2 through StrepTrap and human MPC1 (from membranes provided by supervisors) and MPC2 both with his tags individually purified through IMAC. Above each well there is an explanation of what sample has been loaded. In (a), antibody against his tag has been used and the positive control for his tag is individually purified HuMPC2. In (b), antibody against strep tag has been used and the positive control for strep tag is purified CEHRG4 provided by supervisors. Pictures were generated with a Gel Imaging System (Syngene).

4.3 Proteoliposomes preparation and pyruvate transport activity assay

Human MPC1 alone, MPC2 alone, and MPC1/2 pre-incubated together from individually purified MPC1 and MPC2, was each attempted to be reconstituted into proteoliposomes of asolectin from soybean. Figure 8 illustrates western blots of proteoliposomes reconstituted with MPC1 alone, MPC2 alone and MPC1/2 together. What can be seen is that in all three different sample types, the protein has been successfully incorporated as evidenced by the western blots. In Figure 8d, it can be noticed that the signal from MPC2 in the MPC1/2 proteoliposomes is weaker than the signal from MPC2 in the MPC2 proteoliposomes. The same observation is present in Figure 8e where MPC1 is detected, the MPC1 signal in the MPC1/2 proteoliposomes is weaker than the MPC1 signal in the MPC1 proteoliposomes. The reason for this is that the total moles of protein used in each sample type for the reconstitution was 3 nmol. So, in the heterocomplex MPC1/2, 1.5 nmol of each of MPC1 and MPC2 was used which equalled 3 nmol of protein in total in that sample. In contrast, for the reconstitution of MPC1 alone and MPC2

alone, 3 nmol of MPC1 and MPC2 was used, respectively, that is, the double amount of MPC1 and MPC2 in comparison to their corresponding protein in the heterocomplex sample.

To investigate the pyruvate transport activity of the three different sets of HuMPC complexes, MPC1 alone, MPC2 alone and MPC1/2 together, the proteoliposomes containing the incorporated protein were used in an assay based on the enzymatic reversible conversion of pyruvate and NADH to lactate and NAD^+, respectively, by LDH, in which the absorbance signal of NADH was quantified. So, the principle is that the more pyruvate that has been transported into the proteoliposomes/liposomes, the less pyruvate and also the less NADH can be converted to lactate and NAD^+, respectively, outside the vesicles in the presence of LDH. This will result in a higher absorbance since NADH absorbs significantly at 340 nm, while NAD^+ does not. Figure 8 demonstrate the readings of the absorbance of NADH at 340 nm immediately after the abrogation of the pyruvate transport with the addition of NADH and LDH at the different incubation times. It seems like the proteoliposomes containing HuMPC2 alone has the highest pyruvate transport activity at all three incubation times and is significantly different from the other MPC proteoliposomes. The MPC1 proteoliposomes do not have significantly different pyruvate transport activity in comparison to the empty liposomes (control). The higher absorbance readings for the empty liposomes and MPC1 proteoliposomes in comparison to the liposome-reconstitution buffer without any proteoliposomes/liposomes, could be accounted for that the vesicles are quite leaky so that some pyruvate can still penetrate the lipid bilayer. The inactive HuMPC1 proteoliposomes in this study are in agreement with Nagampalli *et al*. 2018 (*17*) that also demonstrated non-functional HuMPC1 homocomplexes. The researchers in that study discovered as well that HuMPC2 alone can transport pyruvate *in vitro* as an autonomous transporter which agrees with the obtained results here. The HuMPC1/2 proteoliposomes demonstrated significantly higher pyruvate transport in comparison to the empty liposomes at 3 min (Figure 8b) and 5 min (Figure 8c) of incubation time, as well as in comparison to HuMPC1 proteoliposomes at 5 min of incubation time. However, Nagampalli *et al*. 2018 (*17*) demonstrated that HuMPC1/2 could transport pyruvate at similar levels as HuMPC2 alone, but this was not observed in Figure 8 where HuMPC2 has significantly higher pyruvate transport activity compared to HuMPC1/2. This could be accounted for if the situation is such as that MPC1 and MPC2 do not form heterocomplexes in the MPC1/2 proteoliposomes, but instead form only homocomplexes, then the double the amount of MPC2 homocomplexes is present in the MPC2 proteoliposomes in comparison to the MPC1/2 proteoliposomes since the double the amount of MPC2 was used for reconstitution of the MPC2 proteoliposomes for

this assay experiment. This reasoning is based on the assumption that the incorporation efficiency would be equal for all three different MPC proteoliposome sample, which may not be the case in reality. Indeed, as can be seen in Figure 9a-c, the MPC2 proteoliposomes has lower activity than the other MPC proteoliposomes samples which can be accounted for the seemingly lower protein incorporation yield of MPC2 into the MPC2 proteoliposomes (Figure 9d). Furthermore, different from the experiment in Figure 8, 3 nmol of each of MPC1 and MPC2 was used for the reconstitution of the MPC1/2 proteoliposomes for the experiment in Figure 9, so if they form only homocomplexes and not heterocomplexes, the MPC1/2 and MPC2 proteoliposomes should theoretically have had similar pyruvate transport activity if MPC2 had similar incorporation yield in the MPC2 proteoliposomes as the two proteins in the MPC1/2 proteoliposomes. The most possible reason for the lower incorporation of MPC2 in the MPC2 proteoliposomes in Figure 9d could be due to accidentally faulty management during that proteoliposome preparation, since according to Amati *et al.* 2020 (*24*), the lipid composition of the proteoliposomes is the main factor that affects the reconstitution yield of the protein, and the lipid composition has been consistent in all experiments. Furthermore, Amati *et al.* 2020 (*24*) discuss that the orientation of the incorporated protein strongly affects functional studies and is very difficult to influence which often results in a substantial randomisation of the orientation of the protein in the lipid bilayer. This could result in a different amount of preferred/non-preferred orientations of the protein from experiment to experiment, which will make the interpretation of the results more difficult. Even though secondary transporters can shuffle their specific substrate in both directions across the membrane, there might be a difference in the affinity of the substrate on either side of the membrane. Besides the difference in the incorporation yield of the protein in this study, the chances of randomised orientation could be a factor that matters in the interpretation of these results. Indeed, repetitive freeze/thaw cycles when the protein is present (as was performed in this study) have been shown to randomise the protein orientation (*24*), as well as not incorporating the protein into preformed, partially detergent-destabilised liposomes, which was the case here.

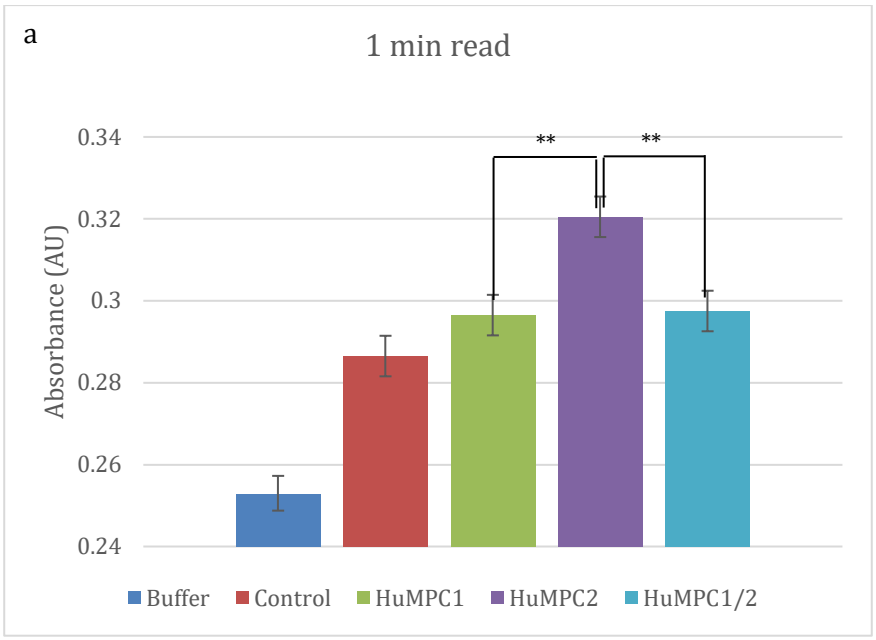
a
1 min read
Absorbance (AU)
0.34
0.32
0.3
0.28
0.26
0.24
**
**
Buffer
Control
HuMPC1
HuMPC2
HuMPC1/2

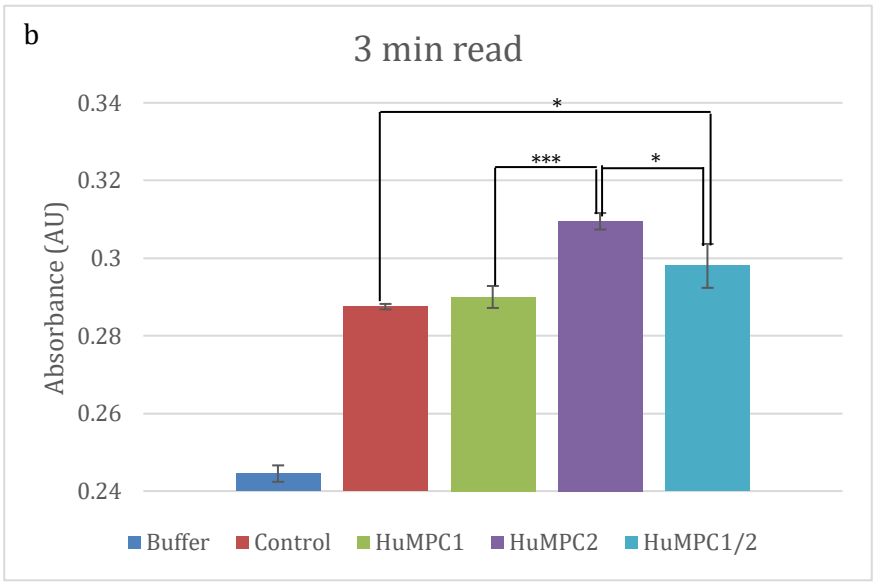
b
3 min read
Absorbance (AU)
0.34
0.32
0.3
0.28
0.26
0.24
*
***
*
Buffer
Control
HuMPC1
HuMPC2
HuMPC1/2

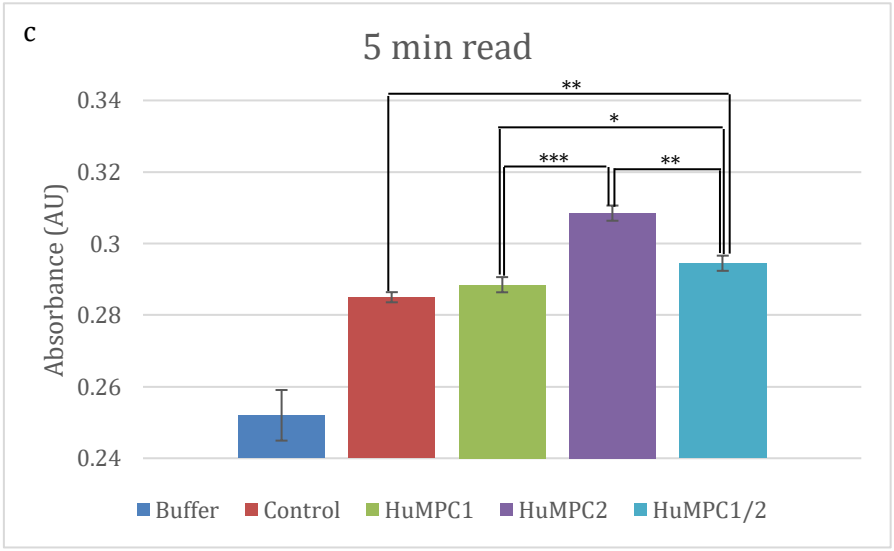
c
5 min read
Absorbance (AU)
0.34
0.32
0.3
0.28
0.26
0.24
**
*
***
**
Buffer
Control
HuMPC1
HuMPC2
HuMPC1/2

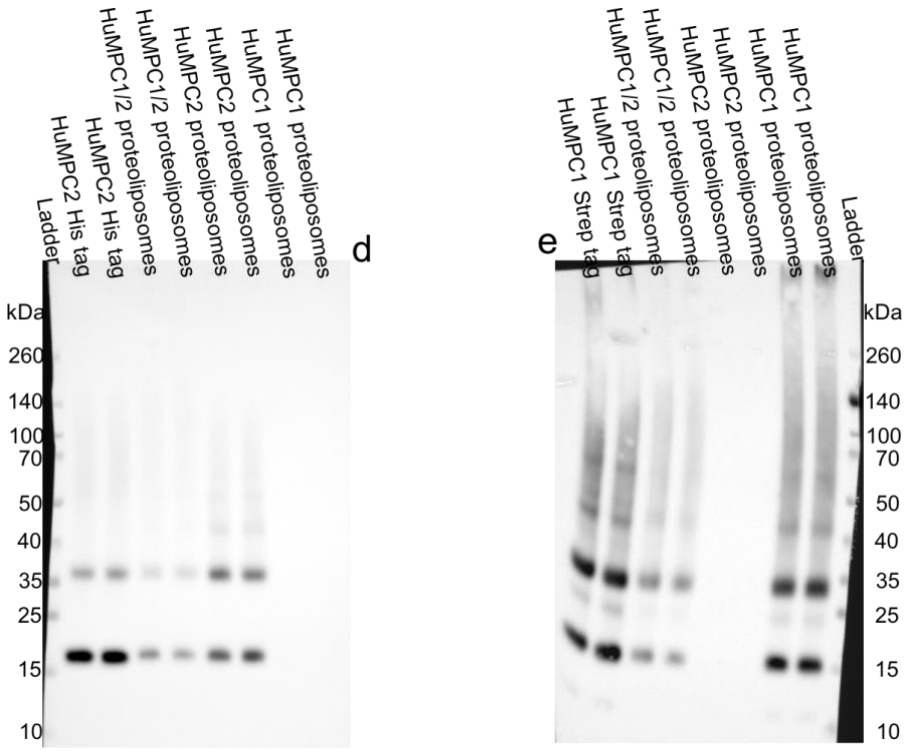

Figure 8: Column charts of obtained readings of the absorbance of NADH at 340 nm immediately after the addition of stop buffer at (a) 1 min, (b) 3 min, and (c) 5 min of incubation time of proteoliposomes/liposomes (from the batch in Figure 8d and 8e) with pyruvate. The y-axis shows the absorbance values (AU), and error bars are also shown for each sample. The colour representation is as follows: blue = liposome-reconstitution buffer without proteoliposomes/liposomes; red = control (empty liposomes); green = proteoliposomes of MPC1; purple = proteoliposomes of MPC2; turquoise = proteoliposomes of heterocomplex MPC1/2. The pyruvate transport activity between the HuMPC proteoliposomes/liposomes was compared with unpaired Student's *t*-tests to obtain *P*-values for the statistically significant level. The asterisks are denoting the following: * at statistically significant level ($0.01 < P \leq 0.05$); ** at very statistically significant level ($0.001 < P \leq 0.01$); *** at extremely statistically significant level ($P \leq 0.001$). Comparisons with no asterisks are not statistically significantly different. The diagrams were generated with Excel. Furthermore, western blots of proteoliposomes reconstituted with human MPC1 alone, MPC2 alone and MPC1/2 together are shown used for this assay experiment. Above each well there is an explanation of what sample has been loaded. In (d), antibody against his tag has been used and the positive control for his tag is individually purified HuMPC2. In (e), antibody against strep tag has been used and the positive control for strep tag is individually purified HuMPC1. The pictures were generated with a Gel Imaging System (Syngene).

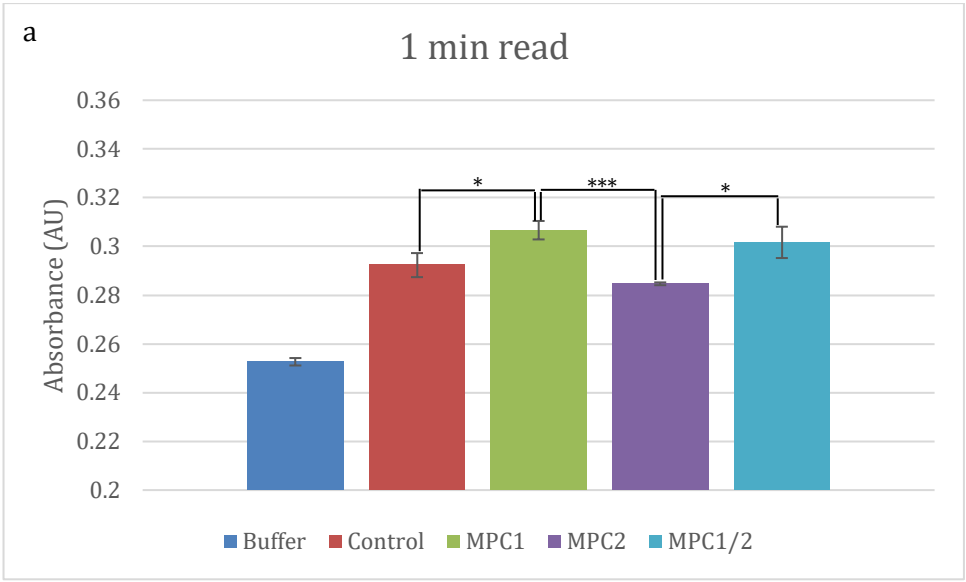
a
1 min read
Absorbance (AU)
0.36
0.34
0.32
0.3
0.28
0.26
0.24
0.22
0.2
*
***
*
Buffer
Control
MPC1
MPC2
MPC1/2

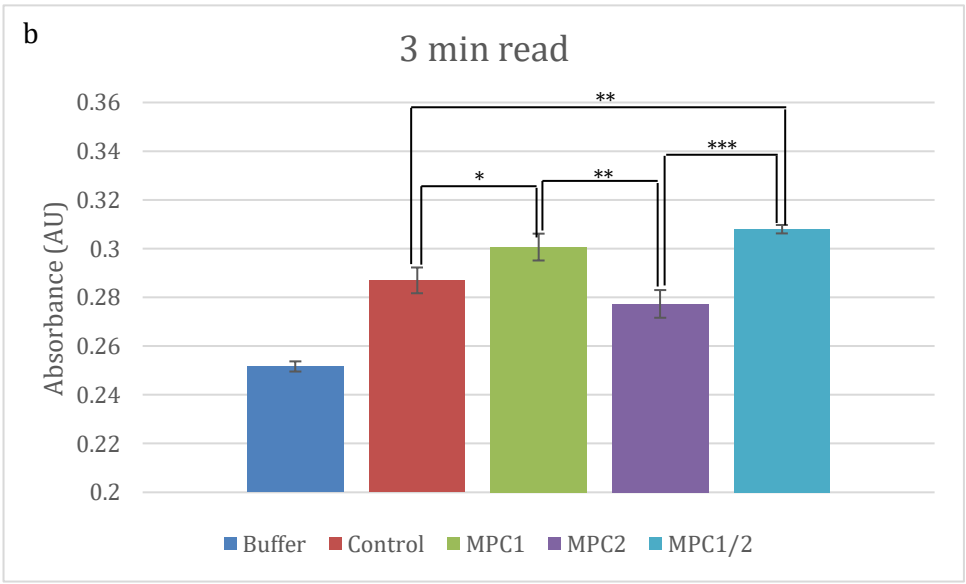
b
3 min read
Absorbance (AU)
0.36
0.34
0.32
0.3
0.28
0.26
0.24
0.22
0.2
**
***
*
**
Buffer
Control
MPC1
MPC2
MPC1/2

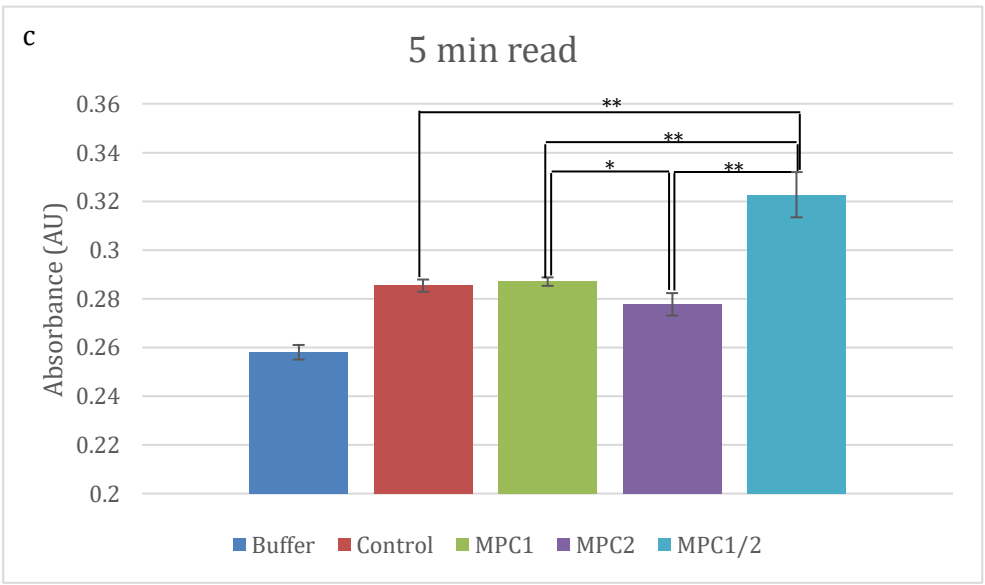
c
5 min read
Absorbance (AU)
0.36
0.34
0.32
0.3
0.28
0.26
0.24
0.22
0.2
**
**
*
**
Buffer
Control
MPC1
MPC2
MPC1/2

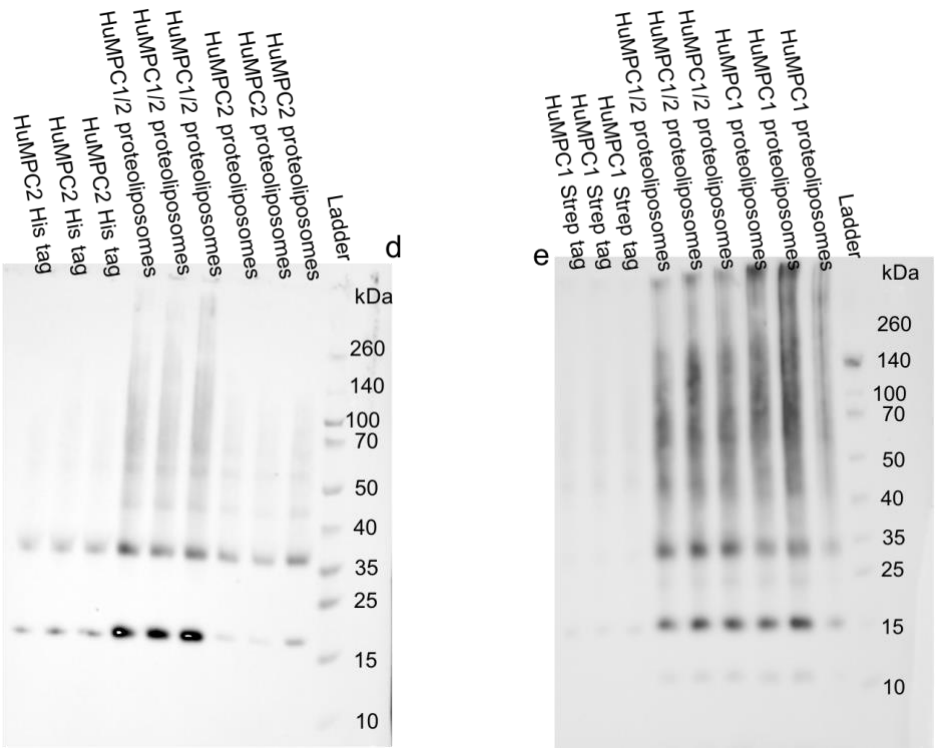

Figure 9: Column charts of obtained readings of the absorbance of NADH at 340 nm immediately after the addition of stop buffer at (a) 1 min, (b) 3 min, and (c) 5 min of incubation time of proteoliposomes/liposomes (from the batch in Figure 9d and 9e) with pyruvate. The y-axis shows the absorbance values (AU), and error bars are also shown for each sample. The colour representation is as follows: blue = liposome-reconstitution buffer without proteoliposomes/liposomes; red = control (empty liposomes); green = proteoliposomes of MPC1; purple = proteoliposomes of MPC2; turquoise = proteoliposomes of heterocomplex MPC1/2. The pyruvate transport activity between the HuMPC proteoliposomes/liposomes was compared with unpaired Student's *t*-tests to obtain *P*-values for the statistically significant level. The asterisks are denoting the following: * at statistically significant level ($0.01 < P \leq 0.05$); ** at very statistically significant level ($0.001 < P \leq 0.01$); *** at extremely statistically significant level ($P \leq 0.001$). Comparisons with no asterisks are not statistically significantly different. The diagrams were generated with Excel. Furthermore, western blots of proteoliposomes reconstituted with human MPC1 alone, MPC2 alone and MPC1/2 together are shown used for this assay experiment. Above each well there is an explanation of what sample has been loaded. In (d), antibody against his tag has been used and the positive control for his tag is individually purified HuMPC2. In (e), antibody against strep tag has been used and the positive control for strep tag is individually purified HuMPC1. The pictures were generated with a Gel Imaging System (Syngene).

4.4 Nano-DSF and mass spectrometry

To prove the existence of a potential HuMPC1/2 heterocomplex in the MPC1/2 proteoliposomes, a temperature stability test in the form of nano-DSF was performed. In Figure 10, curves of the fluorescence ratio at 330 nm/350 nm and its derivative against temperature are shown from the measurement of empty liposomes and the three different types of HuMPC proteoliposomes. See Table 1 in section 8 for the specified onset and melting temperatures from the measurement. It can be noticed that the curves of the ratio at 330 nm/350 nm for the empty liposomes are rather straight, while for the different HuMPC proteoliposomes, some of the curves seem to have a sigmoidal shape, indicating the absence of protein in the empty vesicles. Several studies have demonstrated that the heterocomplex MPC1/2 is more stable than the homocomplexes of MPC1 and MPC2 (*9,15,16*). However, no nano-DSF studies that have been performed on the HuMPC complexes in a lipid environment could be found up until when this report was written. Tavoulari *et al*. 2019 (*10*) performed nano-DSF measurements on the yeast MPC proteins in detergent environment and what can be noticed is that they obtained melting curves that have much more distinct sigmoidal shapes than the ones obtained in this study. Furthermore, Tavoulari *et al*. 2022 (*16*) performed nano-DSF on HuMPC in detergent environment and with different inhibitors, and they also obtained melting curves with much more clear sigmoidal shapes than the ones obtained in this study. This could suggest that when the proteins are imbedded in a lipid bilayer, the proteins seem to be much more thermally stable which can be attributed to the many additional van der Waals interactions with the lipids surrounding the proteins. On the other hand, it could be that the lipidic environment is not applicable for nano-DSF experiments because the lipids may disturb the measurements by affecting the fluorescence of the aromatic residues. Since most of the curves do not have a distinct sigmoidal shape, in fact, only one curve with a clear sigmoidal shape each in Figure 10b and 10d is evident, it is difficult to reason whether a potential HuMPC1/2 heterocomplex is present or absent. Altogether, this must be further investigated.

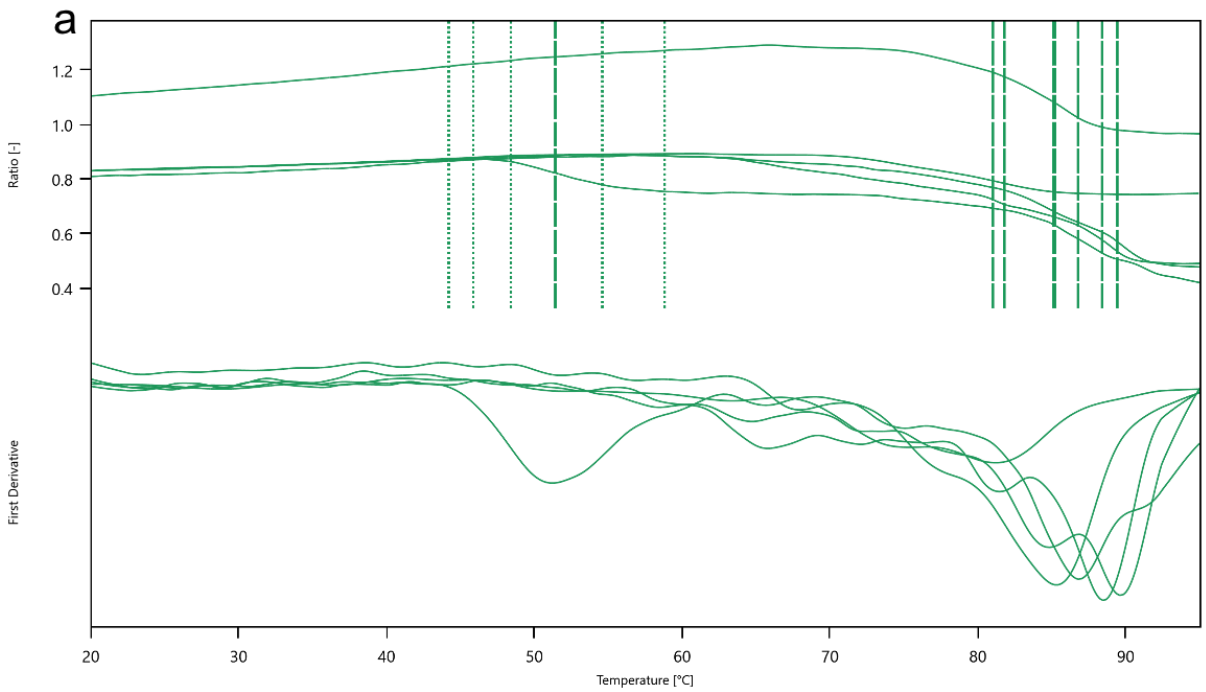
a
Ratio [-]
1.2
1.0
0.8
0.6
0.4
First Derivative
20
30
40
50
60
70
80
90
Temperature [°C]

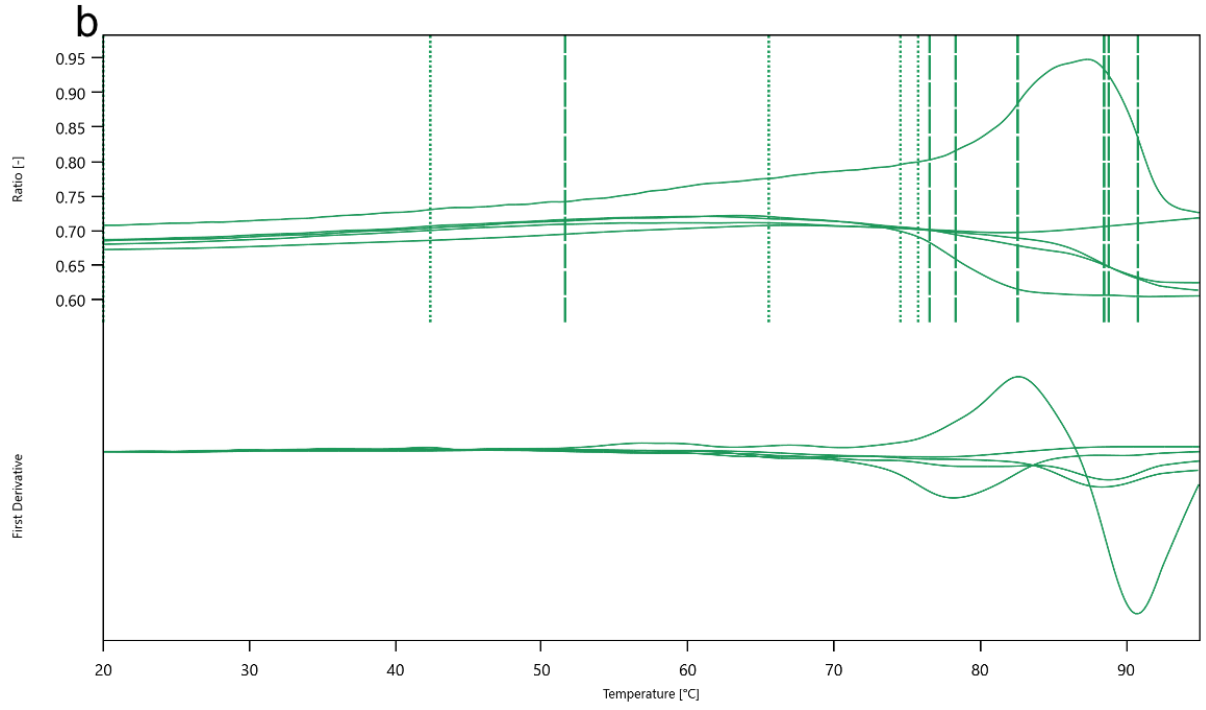
b
Ratio [-]
0.95
0.90
0.85
0.80
0.75
0.70
0.65
0.60
First Derivative
20
30
40
50
60
70
80
90
Temperature [°C]

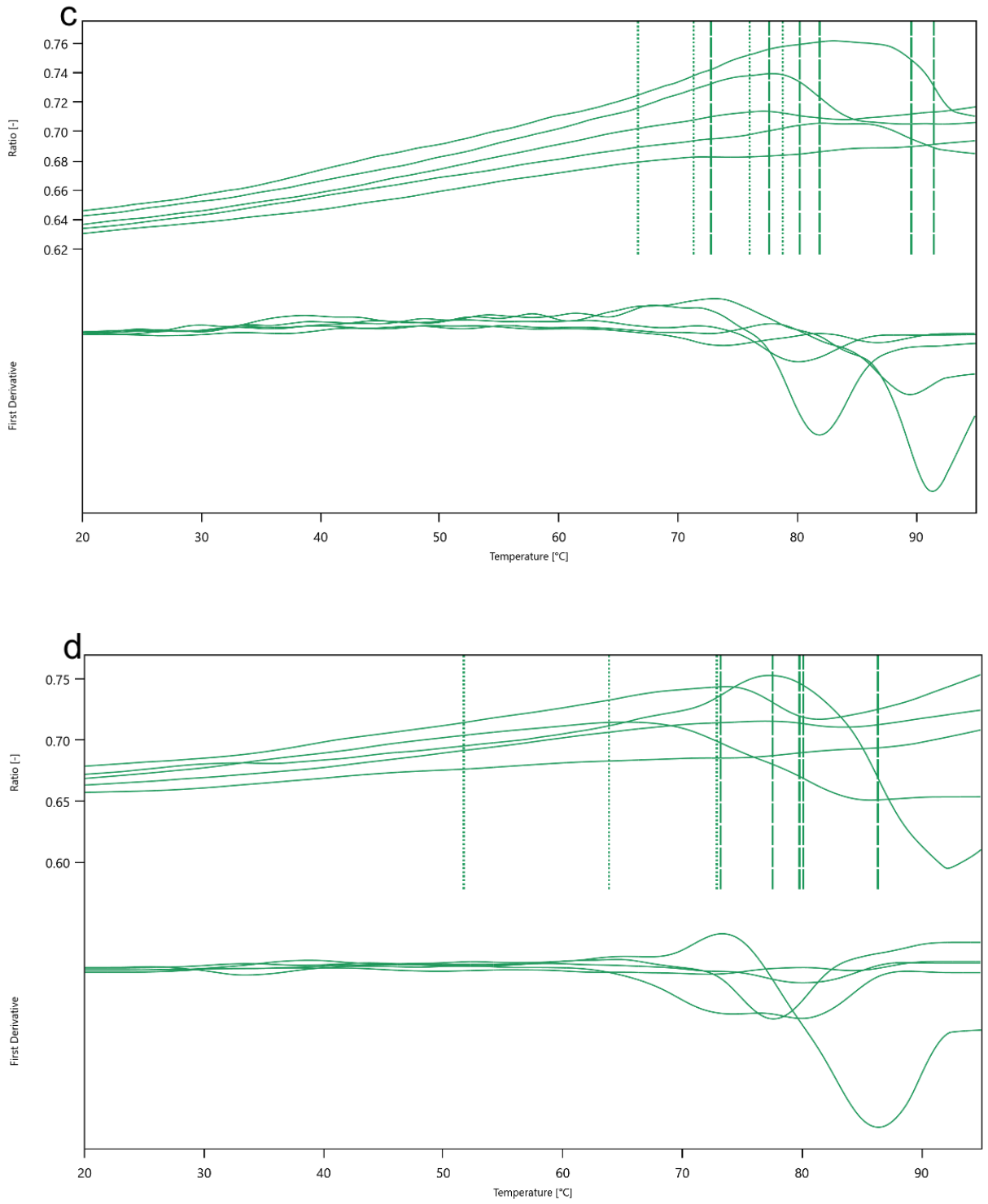

Figure 10: Graphs from the nano-DSF measurement of (a) empty liposomes, (b) HuMPC1, (c) HuMPC2, and (d) HuMPC1/2 proteoliposomes. Five replicates were performed for each sample type. In each graph, the top and bottom y-axes show the fluorescence response of the ratio at 330 nm/350 nm and the first derivative calculated from the changes of fluorescence with temperature, respectively. The x-axis shows the temperature in degrees of Celsius (°C).

For further proof of the existence of the HuMPC1/2 heterocomplex, cross-linking of the MPC1 and MPC2 proteins in the MPC1/2 proteoliposomes was performed for further analysis with mass spectrometry. It was also performed on the MPC1 and MPC2 proteoliposomes. In Figure 11, a silver-stained gel after SDS-PAGE is shown of the cross-linked HuMPC proteoliposome samples as well control samples for each sample type in which no cross-linker was added. It can be seen that no bands are visible for both MPC1 cross-linked and not cross-linked proteoliposome samples which suggests that the concentration of these proteoliposomes were very low and is under the detection limit for silver staining. For the MPC2 cross-linked and not cross-linked proteoliposome samples, bands are only visible in the latter, both the monomer band (blue arrow) at slightly over 15 kDa and the presumably dimer band (green arrow) at slightly over 35 kDa. Notice that in the bottom of the well of MPC2 cross-linked proteoliposome sample, there is substantial detection of protein which suggests that the protein has been unable to migrate through the gel. Furthermore, for both the cross-linked and not cross-linked MPC1/2 proteoliposome samples, bands are visible at same molecular weights as for the MPC2 not cross-linked proteoliposome sample. Same observation is present in the MPC1/2 cross-linked proteoliposome sample where a substantial amount of protein seems to be stuck in the bottom of the well. The reason for this is most likely that the proteins have been cross-linked to the lipids in the proteoliposomes. The cross-linker, DSBU, can cross-link lysine residues (primary amines) and serine, threonine and tyrosine residues (hydroxyl groups) (*26*). The asolectin from soybean used in this study contains a mixture of 25% phosphatidylcholine, 25% phosphatidylethanolamine, 25% phosphatidylinositol, and minor amounts of other phospholipids from soybean. The phosphatidylethanolamine contains a primary amine group that can be subjected to reacting with DSBU. Furthermore, the inositol ring of phosphatidylinositol contains several hydroxyl groups which may also be able to react with DSBU. When the proteins are cross-linked to the lipids, the SDS might not be strong enough to fully denature the proteins which would result in an aggregation type of state that is not able to migrate through the gel. Nagampalli *et al*. 2018 (*17*) performed cross-linking experiments of HuMPC2 alone in isolated native yeast mitochondrial extracts, in detergent environment, and in asolectin-derived proteoliposomes. Interestingly, the authors demonstrated that MPC2 form high order oligomers in a lipid environment while in a detergent environment, the dimeric species was seen as the largest forming complex. Curiously, when MPC2 was cross-linked in the mitochondrial extracts as well as the proteoliposomes, the C-terminal of MPC2 was fused to green fluorescent protein (GFP), while in the detergent environment, free MPC2 was used for cross-linking with no fusion protein. This could advocate for a possible artefact caused by

the GFP in which the GFP-fusion makes it possible for this cross-linking pattern in the lipid environment. It might not be the actual MPC2 that is cross-linked to other MPC2 proteins, but instead the GFP being cross-linked to other GFP or MPC2 proteins. A more consistent approach would be to investigate cross-linking patterns in all three protein environments but with or without a GFP-fusion protein in all three cases, preferably without GFP since that would reflect more the biological environment.

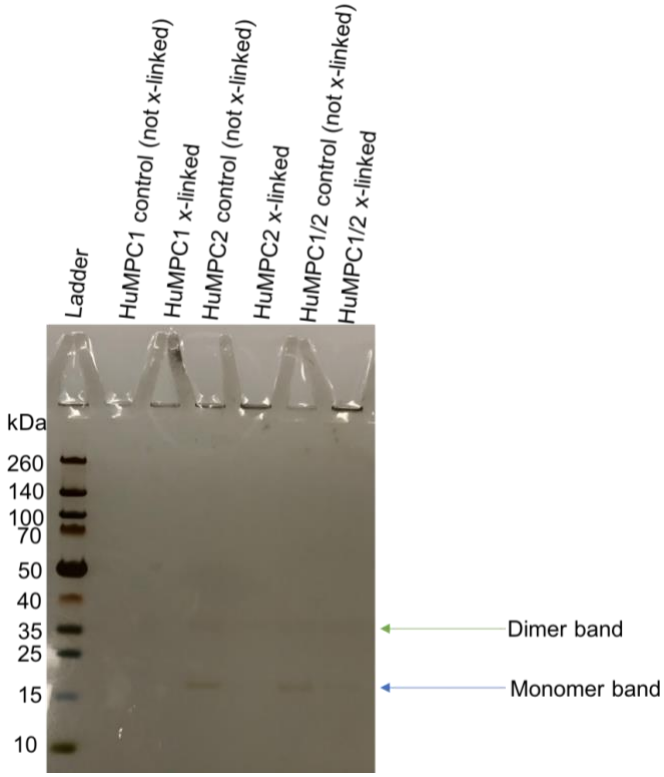

Figure 11: Silver-stained gel after SDS-PAGE of cross-linked HuMPC proteoliposome samples with the cross-linker DSBU. Above each well there is an explanation of what sample has been loaded. A control sample for each HuMPC proteoliposome sample was loaded as well in which no cross-linker was added. The blue and green arrow denote the monomer band and the supposedly dimer band, respectively. Picture was generated with a mobile phone (iPhone 7).

Although the dimer bands are rather faint, an interesting observation is that the ratio of the intensities between the monomer and dimer bands seem to be closer to 1 in the cross-linked MPC1/2 proteoliposome sample in comparison to the not cross-linked sample. Expectations arose that there might be cross-linked proteins present in the dimer band since only the intensity

of the monomer band decreased substantially after cross-linking. After the mass spectrometric analysis, it was found that both human MPC1 and MPC2 was present in the dimer band of cross-linked MPC1/2 proteoliposome sample, however, more peptides of MPC2 could be identified when searching against the Mascot database. This could indicate that MPC2 is more abundant than MPC1 in the MPC1/2 proteoliposomes and if the two proteins were forming a heterocomplex, MPC1 might act like an accessory protein for additional complex stability while MPC2 constitutes the main pyruvate transporting pathway (*18*), and that they do not form a presumed MPC1/2 heterodimer. However, no cross-linked peptides between MPC1 and MPC2 could be identified and very few dead-ends was found which indicates that only a very small fraction of protein has actually been able to react with DSBU. In addition, it is very difficult to extract hydrophobic peptides from gel matrices after in-gel digestion which is a major problem for membrane proteins (*25*). This could be a contributing factor to the limited number of peptides being detected and a solution for this could be to perform in-solution digestion instead. In addition, the suggestion on page 20 in section 4.1 that endogenous MPC subunits from *P. pastoris* might have co-purified with the HuMPC subunits resulting in the prevention of HuMPC complex formation can be confuted since no MPC protein from *P. pastoris* was identified when searching for peptide matches against all protein sequences of *P. pastoris* (who has changed name to *Komagataella pastoris*).

5 Conclusions

With the pyruvate transport activity assay based on the enzymatic activity of LDH, it was shown that the purified human MPC2 alone and MPC1/2 (constituted of separately purified MPC1 and MPC2) displayed functional transport of pyruvate into artificial lipid vesicles. However, which of these two HuMPC complexes is the main functional unit still remains inconclusive. The nano-DSF measurement did not display any concrete hints of the presence of a MPC1/2 heterocomplex and the mass spectrometric analysis after the cross-linking trial did not result in any conclusion of the existence of this heterocomplex. This must be further investigated to generate more established conclusions. Unfortunately, any cryo-EM experiments were not performed due to lack of time so any concluding remarks cannot be applied on the three-dimensional structure of the HuMPC complex.

6 Future aspects

First and foremost, work remains to be done on the three-dimensional structure of the HuMPC complex since no such experiments were performed in this study due to lack of time. Furthermore, one can try to optimise the proteoliposome preparation to generate populations of a more consistent orientation of the protein in the lipid bilayer in order to minimise complications around interpreting the results from the pyruvate transport activity assay. This could include incorporating the protein into preformed, partially detergent-destabilised liposomes, as Steffen *et al*. 2022 (*22*) did on working with aquaporins. In addition, one could also quantify the incorporation yield into the proteoliposomes by using an image processing program in which intensities of the proteoliposomes on the western blot are compared to the intensity of a known amount of protein on the same blot. This would eliminate any ambiguity in the interpretation of the results by relating the incorporation yield of the protein with its respective activity. This was tried with ImageJ during this master thesis project but chosen to not be included in the final report because of incorrectly processing of the image and overexposed western blots. The leakiness of the proteoliposomes/liposomes could be repaired with the addition of cholesterol which have been shown to impact the tightness of liposomal membranes (*27*). Furthermore, one can perform analytical size exclusion chromatography (SEC) to investigate the apparent molecular weight of the human MPC1/2 complex. However, one has to first optimise the co-purification of the MPC1/2 complex in which other detergents with smaller micelles could be tested. Lastly, one could attempt to solubilise the proteins in the proteoliposomes with a mild detergent, such as DDM, and subsequently perform the nano-DSF measurement and investigate if that can give more concrete conclusions. This is assuming that nothing is happening to the apparent complexes when changing their environment from lipids to detergents. Furthermore, another cross-linker could be tested that does not react with any lipids and see if that could solve the cross-linking issue, as well as scaling up the reaction. Alternatively, one could use other kinds of lipids that does not contain these reactive groups towards DSBU.

7 References

1. Patterson, J. N.; Cousteils, K.; Lou, J. W.; Manning Fox, J. E.; MacDonald, P. E.; Joseph, J. W., Mitochondrial metabolism of pyruvate is essential for regulating glucose-stimulated insulin secretion. J Biol Chem 2014, 289 (19), 13335-46.

2. Vander Heiden, M. G.; Cantley, L. C.; Thompson, C. B., Understanding the Warburg effect: the metabolic requirements of cell proliferation. Science 2009, 324 (5930), 1029-33.

3. Ghosh, A.; Tyson, T.; George, S.; Hildebrandt, E. N.; Steiner, J. A.; Madaj, Z.; Schulz, E.; Machiela, E.; McDonald, W. G.; Escobar Galvis, M. L.; Kordower, J. H.; Van Raamsdonk, J. M.; Colca, J. R.; Brundin, P., Mitochondrial pyruvate carrier regulates autophagy, inflammation, and neurodegeneration in experimental models of Parkinson's disease. Sci Transl Med 2016, 8 (368), 368ra174.

4. Buchanan, J. L.; Taylor, E. B., Mitochondrial Pyruvate Carrier Function in Health and Disease across the Lifespan. Biomolecules 2020, 10 (8).

5. Rauckhorst, A. J.; Taylor, E. B., Mitochondrial pyruvate carrier function and cancer metabolism. Curr Opin Genet Dev 2016, 38, 102-109.

6. Zangari, J.; Petrelli, F.; Maillot, B.; Martinou, J. C., The Multifaceted Pyruvate Metabolism: Role of the Mitochondrial Pyruvate Carrier. Biomolecules 2020, 10 (7).

7. Bricker, D. K.; Taylor, E. B.; Schell, J. C.; Orsak, T.; Boutron, A.; Chen, Y. C.; Cox, J. E.; Cardon, C. M.; Van Vranken, J. G.; Dephoure, N.; Redin, C.; Boudina, S.; Gygi, S. P.; Brivet, M.; Thummel, C. S.; Rutter, J., A mitochondrial pyruvate carrier required for pyruvate uptake in yeast, Drosophila, and humans. Science 2012, 337 (6090), 96-100.

8. Herzig, S.; Raemy, E.; Montessuit, S.; Veuthey, J. L.; Zamboni, N.; Westermann, B.; Kunji, E. R.; Martinou, J. C., Identification and functional expression of the mitochondrial pyruvate carrier. Science 2012, 337 (6090), 93-6.

9. Xu, L.; Phelix, C. F.; Chen, L. Y., Structural Insights into the Human Mitochondrial Pyruvate Carrier Complexes. J Chem Inf Model 2021, 61 (11), 5614-5625.

10. Tavoulari, S.; Thangaratnarajah, C.; Mavridou, V.; Harbour, M. E.; Martinou, J. C.; Kunji, E. R., The yeast mitochondrial pyruvate carrier is a hetero-dimer in its functional state. Embo j 2019, 38 (10).

11. Crichton, P. G.; Harding, M.; Ruprecht, J. J.; Lee, Y.; Kunji, E. R., Lipid, detergent, and Coomassie Blue G-250 affect the migration of small membrane proteins in blue native gels: mitochondrial carriers migrate as monomers not dimers. J Biol Chem 2013, 288 (30), 22163-73.

12. Halestrap, A. P., Pyruvate and ketone-body transport across the mitochondrial membrane. Exchange properties, pH-dependence and mechanism of the carrier. Biochem J 1978, 172 (3), 377-87.

13. Halestrap, A. P., The mitochondrial pyruvate carrier. Kinetics and specificity for substrates and inhibitors. Biochem J 1975, 148 (1), 85-96.

14. Divakaruni, A. S.; Wiley, S. E.; Rogers, G. W.; Andreyev, A. Y.; Petrosyan, S.; Loviscach, M.; Wall, E. A.; Yadava, N.; Heuck, A. P.; Ferrick, D. A.; Henry, R. R.; McDonald, W. G.; Colca, J. R.; Simon, M. I.; Ciaraldi, T. P.; Murphy, A. N., Thiazolidinediones are acute, specific inhibitors of the mitochondrial pyruvate carrier. Proc Natl Acad Sci U S A 2013, 110 (14), 5422-7.

15. Lee, J.; Jin, Z.; Lee, D.; Yun, J. H.; Lee, W., Characteristic Analysis of Homo- and Heterodimeric Complexes of Human Mitochondrial Pyruvate Carrier Related to Metabolic Diseases. Int J Mol Sci 2020, 21 (9).

16. Tavoulari, S.; Schirris, T. J. J.; Mavridou, V.; Thangaratnarajah, C.; King, M. S.; Jones, D. T. D.; Ding, S.; Fearnley, I. M.; Kunji, E. R. S., Key features of inhibitor binding to the human mitochondrial pyruvate carrier hetero-dimer. Mol Metab 2022, 60, 101469.

17. Nagampalli, R. S. K.; Quesñay, J. E. N.; Adamoski, D.; Islam, Z.; Birch, J.; Sebinelli, H. G.; Girard, R.; Ascenção, C. F. R.; Fala, A. M.; Pauletti, B. A.; Consonni, S. R.; de Oliveira, J. F.; Silva, A. C. T.; Franchini, K. G.; Leme, A. F. P.; Silber, A. M.; Ciancaglini, P.; Moraes, I.; Dias, S. M. G.; Ambrosio, A. L. B., Human mitochondrial pyruvate carrier 2 as an autonomous membrane transporter. Sci Rep 2018, 8 (1), 3510.

18. Quesñay, J. E. N.; Pollock, N. L.; Nagampalli, R. S. K.; Lee, S. C.; Balakrishnan, V.; Dias, S. M. G.; Moraes, I.; Dafforn, T. R.; Ambrosio, A. L. B., Insights on the Quest for the Structure-Function Relationship of the Mitochondrial Pyruvate Carrier. Biology (Basel) 2020, 9 (11).

19. Xu, Y.; Tao, Y.; Cheung, L. S.; Fan, C.; Chen, L. Q.; Xu, S.; Perry, K.; Frommer, W. B.; Feng, L., Structures of bacterial homologues of SWEET transporters in two distinct conformations. Nature 2014, 515 (7527), 448-452.

20. Bender, T.; Pena, G.; Martinou, J. C., Regulation of mitochondrial pyruvate uptake by alternative pyruvate carrier complexes. Embo j 2015, 34 (7), 911-24.

21. Li, L.; Wen, M.; Run, C.; Wu, B.; OuYang, B., Experimental Investigations on the Structure of Yeast Mitochondrial Pyruvate Carriers. Membranes (Basel) 2022, 12 (10).

22. Steffen, J. H.; Missel, J. W.; Al-Jubair, T.; Kitchen, P.; Salman, M. M.; Bill, R. M.; Törnroth-Horsefield, S.; Gourdon, P., Assessing water permeability of aquaporins in a proteoliposome-based stopped-flow setup. STAR Protoc 2022, 3 (2), 101312.

23. Brunelle, E.; Le, A. M.; Huynh, C.; Wingfield, K.; Halámková, L.; Agudelo, J.; Halámek, J., Coomassie Brilliant Blue G-250 Dye: An Application for Forensic Fingerprint Analysis. Anal Chem 2017, 89 (7), 4314-4319.

24. Amati, A. M.; Graf, S.; Deutschmann, S.; Dolder, N.; von Ballmoos, C., Current problems and future avenues in proteoliposome research. Biochem Soc Trans 2020, 48 (4), 1473-1492.

25. Alfonso-Garrido, J.; Garcia-Calvo, E.; Luque-Garcia, J. L., Sample preparation strategies for improving the identification of membrane proteins by mass spectrometry. Anal Bioanal Chem 2015, 407 (17), 4893-905.

26. Yılmaz, Ş.; Busch, F.; Nagaraj, N.; Cox, J., Accurate and Automated High-Coverage Identification of Chemically Cross-Linked Peptides with MaxLynx. Anal Chem 2022, 94 (3), 1608-1617.

27. Nakhaei, P.; Margiana, R.; Bokov, D. O.; Abdelbasset, W. K.; Jadidi Kouhbanani, M. A.; Varma, R. S.; Marofi, F.; Jarahian, M.; Beheshtkhoo, N., Liposomes: Structure,

Biomedical Applications, and Stability Parameters With Emphasis on Cholesterol. Front Bioeng Biotechnol 2021, 9, 705886.

8 Appendix

Table 1: Onset temperatures and temperatures for inflection point #1 and #2 from nano-DSF of HuMPC1, HuMPC2 and HuMPC1/2 proteoliposomes. Five replicates were performed for each sample type. ND = not detected. Temperatures are not given for the empty liposomes since the curves in Figure 10a are rather straight.

Sample type	Onset temperature (°C)	Inflection point #1 (°C)	Inflection point #2 (°C)
HuMPC1 proteoliposomes	20.0; 65.6; 74.5; 75.7; 42.4	51.7; 78.3; 82.6; 88.4; 88.8	76.6; ND; 90.8; ND; ND
HuMPC2 proteoliposomes	78.8; ND; 71.4; 66.7; 76.0	81.9; 77.7; 80.2; 72.8; 81.9	ND; 89.6; ND; 91.5; ND
HuMPC1/2 proteoliposomes	ND; ND; 51.8; 72.9; 63.8	80.2; ND, 73.2; 77.6; 79.8	ND; ND; 86.4; ND; ND